Excitation of Cortical nNOS/NK1R Neurons by Hypocretin 1 is Independent of Sleep Homeostasis

Rhîannan H Williams, Sarah W Black, Alexia M Thomas, Juliette Piquet, Bruno Cauli, Thomas S Kilduff

HAL Id: hal-02168362
https://hal.sorbonne-universite.fr/hal-02168362v1

Submitted on 28 Jun 2019

Excitation of Cortical nNOS/NK1R Neurons by Hypocretin 1

Is Independent of Sleep Homeostasis

Rhîannan H. Williams[1,2], Sarah W Black[1,#], Alexia M. Thomas[1], Juliette Piquet[3],

Bruno Cauli[3] and Thomas S. Kilduff[1]

[1]Center for Neuroscience, Biosciences Division, SRI International,

Menlo Park, CA 94025, USA

[2] Institute for Neurogenomics, Helmholtz Zentrum München, German Research Centre

for Environmental Health, Neuherberg, 85764, Germany

[3] Sorbonne Universités, UPMC Univ Paris 06, INSERM, CNRS, Neuroscience Paris

Seine - Institut de Biologie Paris Seine (NPS - IBPS), 75005 Paris, France

Running Title: Cortical nNOS/NK1R neurons respond to HCRT1

Figures: 7   Tables: 3

#Current Address: Reset Therapeutics, 260 Littlefield Ave #200, South San Francisco,

CA 94080

* Corresponding Author:

Dr. Thomas Kilduff, Center for Neuroscience, Biosciences Division, SRI International,

333 Ravenswood Avenue, Menlo Park, CA 94025, USA; E-mail: thomas.kilduff@sri.com

Abstract

We have proposed that cortical nNOS/NK1R interneurons have a role in sleep homeostasis. The hypocretins (orexins) are wake-promoting neuropeptides and hypocretin/orexin (Hcrt) neurons project to the cortex. Hcrt peptides affect deep layer cortical neurons, and Hcrt receptor 1 (*Hcrtr1; Ox1r*) mRNA is expressed in cortical nNOS/NK1R cells. Therefore, we investigated whether Hcrt neuron stimulation affects cingulate cortex nNOS/NK1R neurons. Bath application of HCRT1/orexin-A evoked an inward current and membrane depolarization in most nNOS/NK1R cells which persisted in tetrodotoxin; optogenetic stimulation of Hcrt terminals expressing channelrhodopsin-2 confirmed these results, and pharmacological studies determined that HCRTR1 mediated these responses. Single cell RT-PCR found *Hcrtr1* mRNA in 31% of nNOS/NK1R cells without any *Hcrtr2* mRNA expression; immunohistochemical studies of *Hcrtr1-EGFP* mice confirmed that a minority of nNOS/NK1R cells express HCRTR1. When Hcrt neurons degenerated in *orexin-tTA;TetO DTA* mice, the increased EEG delta power during NREM sleep produced in response to 4 h sleep deprivation and c-FOS expression in cortical nNOS/NK1R cells during recovery sleep were indistinguishable from that of controls. We conclude that Hcrt excitatory input to these deep layer cells is mediated through HCRTR1 but is unlikely to be involved in the putative role of cortical nNOS/NK1R neurons in sleep homeostasis.

Keywords: arousal, hypocretin, nitric oxide, sleep, wakefulness

Introduction

Cortical GABAergic interneurons have been classified using morphological, neurochemical and electrophysiological criteria (Ascoli et al. 2008; DeFelipe et al. 2013) and, more recently, on the basis of single cell transcriptomic data (Zeisel et al. 2015; Tasic et al. 2016). Using neurochemical criteria, neurons that co-express neuronal nitric oxide synthase (nNOS) and the neurokinin-1 receptor (NK1R) comprise the rarest currently known type of cortical interneuron (Kubota et al. 2011). Transcriptomic studies also indicate that cortical nNOS/NK1R interneurons, which are primarily found in the deep layers of the cerebral cortex, are a unique subpopulation of somatostatin/neuropeptide Y cells (Tasic et al. 2016). Cortical nNOS/NK1R neurons correspond to Type I nNOS cells and are unique among GABAergic interneurons in having long-range intracortical projections (Tomioka et al. 2005; Higo et al. 2007; Tomioka and Rockland 2007; Higo et al. 2009). Type I nNOS cells can be distinguished from the more numerous Type II nNOS cells on the basis of soma size and the intensity of staining for both nNOS and the NADPH diaphorase (Yan and Garey 1997).

In contrast to other cortical neurons, Type I nNOS cells accumulate Fos protein during sleep but not during wakefulness (Gerashchenko et al. 2008; Pasumarthi et al. 2010; Morairty et al. 2013). The proportion of nNOS cells that express Fos during sleep is proportional to the homeostatic sleep drive that accumulates during wakefulness (Morairty et al. 2013; Dittrich et al. 2015). Mice lacking nNOS have altered electroencephalographic (EEG) activity during both wakefulness and sleep, with greater EEG spectral power in the delta (0.5-4Hz) range during wakefulness and a deficit in the

low delta range of slow wave activity (0.5-2.5Hz) during sleep; these nNOS knockout mice also have a greatly attenuated homeostatic response to sleep deprivation (Morairty et al. 2013). However, even in the absence of nNOS, cortical NK1R neurons express Fos during sleep, suggesting that Fos production in these cells is likely due to afferent activation of these cells rather than to the presence of nNOS *per se* (Morairty et al. 2013). Based on these observations, we have proposed that Type I cortical nNOS cells (i.e., nNOS/NK1R neurons) play a critical role in coupling homeostatic sleep drive (presumably, of subcortical origin) to EEG slow wave activity and suggested a model in which these cells are inactivated during wakefulness and activated during sleep based on putative afferent inputs (Kilduff et al. 2011).

The hypocretin/orexin (Hcrt) neuropeptides are well known to be involved in the regulation of wakefulness. Hcrt terminals innervate the deep layers of the cerebral cortex (Peyron et al. 1998) and a subpopulation of layer VIb cortical neurons respond to application of Hcrt peptides (Hay et al. 2015; Wenger Combremont et al. 2016a). Single cell transcriptomic studies have revealed that about half of cortical nNOS/NK1R interneurons express hypocretin receptor 1 (*Hcrtr1*) mRNA (Tasic et al. 2016). Consequently, we evaluated whether cortical nNOS/NK1R neurons respond to HCRT1 and whether Hcrt input to these cells could play a role in homeostatic sleep regulation. We find that cortical nNOS/NK1R neurons receive Hcrt input and that HCRT1/orexin-A application affects the excitability of a subset of cortical nNOS/NK1 neurons *in vitro* but the absence of this input does not affect the ability of cortical nNOS/NK1 neurons to detect sleep pressure *in vivo*.

Materials and Methods

Animals

All rodents were maintained under 12 h light : 12 h dark conditions at 22 ± 2°C and 50 ± 25% relative humidity with food and water *ad libitum* and were treated in accordance with guidelines from the NIH *Guide for the Care and Use of Laboratory Animals.* All protocols were approved by SRI International's Institutional Animal Care and Use Committee. Table 1 lists the 8 strains of mice used in this study. C57Bl/6J mice (Jackson Laboratories strain #000664; RRID:IMSR_JAX:000664) were used for *in vitro* electrophysiological slice recordings (P13-28, male and female). *nNOS-CreER;Ai14* mice were produced by crossing *nNOS-CreER* (B6;129S-*Nos1$^{tm1.1(cre/ERT2)Zjh}$*/J; Jackson Laboratories strain #014541; RRID:IMSR_JAX:014541) (Taniguchi et al. 2011) and Ai14 mice (B6;129S6-*Gt(ROSA)26Sor$^{tm14(CAG-tdTomato)Hze}$*/J; Jackson Laboratories strain #007914; RRID:IMSR_JAX:007914) (Madisen et al. 2010). This bigenic strain was crossed with *Orexin-tTA* mice (*ox-tTA*) mice (Tabuchi et al. 2013) to produce trigenic *ox-tTA;nNOS-CreER;Ai14* mice that were used for optogenetic experiments (>8 weeks of age, male and female). *Orexin-tTA;TetO diptheria toxin A fragment* (DTA) mice (Tabuchi et al. 2014) were used to selectively degenerate Hcrt neurons after removal of doxycycline (DOX) from the chow; these mice were used for *in vitro* electrophysiological slice recordings (P14-23, male and female; parents were maintained as DOX(-)), histological analysis (P14-23, male and female), and EEG recordings (>42 weeks old, male, DOX(-) for 22 wks at time of sacrifice). Age-matched monogenic littermates were used as controls for EEG studies. Lastly, brains from *Hcrtr1-EGFP* mice (RRID:MMRRC_030803-UCD) (Darwinkel et al.

2014; Ch'ng and Lawrence 2015), used exclusively for immunohistochemical studies, were obtained from Professor Paul Kenny, Mount Sinai, New York.

Stereotaxic injections

Expression of channelrhodopsin (ChR2) in Hcrt neurons of the lateral hypothalamic area (LHA). Male and female *ox-tTA;nNOS-CreER;Ai14* mice (8-11 week old; *n* = 8) were anesthetized with isoflurane (5% induction, 1-2% maintenance) and shaved to remove hair from the head. Mice were placed in a stereotactic frame (David Kopf Instruments, Tujunga, CA) and body temperature was regulated with a heating pad (37°C; T/pump, Gaymar Industries, Orchard Park, NY). The surgical site was disinfected with three alternating washes of 2% chlorohexidine gluconate diluted 1:50 (Henry Schein, Dublin, OH) and sterile water before a cranial incision was made. Using a pulled glass micropipette (Harvard Apparatus, Holliston, MA) and Picospritzer II (Parker Hannifin, Pine Brook, NJ), we bilaterally microinjected 200 nl (at a rate 40 nl/min) of the adeno-associated viral (AAV) vector AAV(DJ)-TetO-ChR2(ET/TC)-eYFP (from Prof. Akihiro Yamanaka, Nagoya University) into the tuberal hypothalamus at coordinates of AP-1.5mm, ML±0.74mm, DV5.1mm (Franklin and Paxinos 2008). This AAV encodes the blue light-sensitive ChR2 under control of TetO. The pipette was withdrawn from the tissue 5 min following each injection. The skin was sutured and mice were returned to their home cage. Analgesic administration of buprenorphine (0.05-0.1 mg/kg), meloxicam (5 mg/kg) and bupivacaine (2 mg/kg) was used pre- or post-surgery. Three weeks after AAV injections, we injected tamoxifen (75 mg/kg, *i.p.*) to induce Cre expression in nNOS neurons. Mice were 12-15 weeks old when they

were sacrificed for *in vitro* optogenetic studies. To assess viral expression and transduction efficiency, *ox-tTA* or wild type (WT) littermate mice were injected following the protocol described above (*n* = 2; male and female). These mice did not receive a tamoxifen injection and, 4 weeks after intracranial injection, were deeply anesthetized (see below), perfused transcardially, and the brain removed for histological processing.

Immunohistochemistry and cell counting

Except for *Hcrtr1-EGFP* mice, all mice sacrificed for histological examination received a terminal injection of SomnaSol (Henry Schein, Dublin, OH) before being transcardially perfused with PBS and heparin followed by 4% PFA. After removal of the brain, the tissue was cryprotected (30% sucrose, 0.1 M PB solution) and cut into six series of 30 µm thick coronal sections in preparation for immunohistochemical processing.

Antibody characterization. The specificity of the primary goat anti-neuronal nitric oxide antibody (nNOS; Abcam Cat# ab1376; RRID:AB_300614), chicken anti-GFP (Abcam Cat# ab13970; RRID:AB_300798) and secondary antibodies were tested as previously mentioned (Williams et al. 2017). The anti-orexin-A (Santa Cruz Biotechnology Cat# sc-8070; RRID:AB_653610) and anti-orexin-B (Santa Cruz Biotechnology Cat# sc-8071; RRID:AB_653612) antisera are listed in the antibody registry database (http://antibodyregistry.org/).

Hcrtr1-EGFP mice. Paraformaldehyde-fixed brain tissue was cut into 6 series of 30 µm thick coronal sections. One series of four sections from an adult male mouse was then processed in chicken anti-GFP (1:2000, Abcam Cat# ab13970;

RRID:AB_300798) and goat anti-nNOS (1:3000, Abcam Cat# ab1376; RRID:AB_300614). The secondary antibodies used were Alexa Fluor 488 affiniPure donkey anti-chicken IgY (for GFP; 1:1000, 1 h; Jackson ImmunoResearch; RRID:AB_2340375) and Alexa Fluor® 594 affiniPure donkey anti-goat IgG (1:500, Jackson ImmunoResearch).

Channelrhodopsin-2 expression in ox-tTA mice. Four weeks after bilateral injection of AAV(DJ)-TetO-ChR2(ET/TC)-eYFP into the tuberal hypothalamus, mice (1 *ox-tTA* male; 1 WT male, both 10 wks of age) were perfused and brain tissue prepared. One series of four sections from each mouse was then processed with anti-orexin-A (1:3000, Santa Cruz Biotechnology Cat# sc-8070; RRID:AB_653610) and anti-orexin-B (1:3000, Santa Cruz Biotechnology Cat# sc-8071; RRID:AB_653612) antisera to detect Hcrt-expressing cell bodies before secondary detection with Alexa Fluor® 546 affiniPure donkey anti-goat IgG (1:1000, Jackson ImmunoResearch). To detect ChR2-expressing neurons, we used chicken anti-GFP (detects ChR2-eYFP, 1:1000, Abcam Cat# ab13970; RRID:AB_300798) and then Alexa Fluor® 594 affiniPure donkey anti-goat IgG (1:500, Jackson ImmunoResearch). Transduction efficiency of the ChR2-eGFP virus within the Hcrt field was calculated by counting the number of ChR2-eGFP[+]/HCRT1&2-immunoreactive (ir)[+] cells and the total number of HCRT1&2-ir[+] cell bodies and then calculating the percentage of double-labelled cells relative to the total number of Hcrt neurons. Transduction specificity was calculated as the proportion of GFP-ir^{+} cells that co-expressed HCRT1&2-ir[+] relative to the total number of GFP-ir^{+} cells. The region measured included all HCRT1&2-ir[+] cell bodies within the tuberal hypothalamus in the sections used for immunohistochemical quantification (Bregma: -1.34mm – -1.58mm)

(Franklin and Paxinos 2008). Subsequent histological analysis revealed that the vast

majority of transfected cells were within the lateral hypothalamic area (LHA), although

some were medial to the fornix. For simplicity, we refer below to the transfected cells as

from the LHA.

Hcrt neuron degeneration in DTA mice. We calculated Hcrt neuron

degeneration in juvenile (male and female, P21-27) mice removed from doxycycline

(DOX(-); *n* = 4) with age-matched DOX(+) mice (male and female, P21-28; *n* = 3). One

series of four sections from each mouse was processed in anti-orexin-A (1:3000, Santa

Cruz Biotechnology Cat# sc-8070; RRID:AB_653610) and anti-orexin-B (1:3000, Santa

Cruz Biotechnology Cat# sc-8071; RRID:AB_653612) antisera to detect Hcrt-expressing

cell bodies before secondary detection with Alexa Fluor® 546 affiniPure donkey anti-goat

IgG (1:1000, Jackson ImmunoResearch). Two bilateral sections, per mouse, of the

medial Hcrt-expressing field within the tuberal hypothalamus were taken for cell counts

(Bregma: -1.34mm to -1.56mm) (Franklin and Paxinos 2008). The *ox-tTA;TetO-DTA*

("DTA") mice and monogenic controls used in EEG studies were sacrificed at either

ZT4-4.5 (SD group) or ZT5.75-6.25 (RS group). Six sections from one series that

included the cingulate cortex were processed with rabbit anti-c-FOS (1:3000, Santa

Cruz Biotechnology Cat# sc-52; RRID:AB_2106783) and goat anti-nNOS (1:3000,

Abcam Cat# ab1376; RRID:AB_300614). Secondary antibodies used were donkey

anti-rabbit IgG (1:1000, Jackson ImmunoResearch; RRID:AB_2340584) and donkey

anti-goat IgG (1:1000, Abcam Cat# ab13970; RRID: AB_300798). C-FOS was detected

with nickel-enhanced 3,3′ diaminobenzidine tetrahydrochloride (nDAB; 10 min; SK4100,

Vector Laboratories) and nNOS with 3,3′ diaminobenzidine tetrahydrochloride (DAB; 4

9

min; SK4100, Vector Laboratories). The number of nNOS neurons and the number of

nNOS cells colocalizing with c-FOS throughout the cortex, excluding the piriform, were

counted (Bregma: 1.2mm to + 0.86mm) (Franklin and Paxinos 2008). The percentage

of colocalized nNOS cells per mouse was calculated and the grouped data expressed

as mean ± SEM.

Post-recording verification of cell phenotype. For cells collected for scRT-PCR,

slices were post-fixed in 4% PFA before processing for biocytin and nNOS. Thick

sections (250 μm) were incubated overnight in goat anti-nNOS (1:1000, Abcam Cat#

ab1376; RRID:AB_300614) and then Alexa Fluor® 594 affiniPure donkey anti-goat IgG

(1:1000, 2h; Jackson ImmunoResearch) with streptavidin-conjugated fluorescein

(DTAF; for biocytin; 1:500, 2h; Jackson ImmunoResearch). Sections were mounted

using Pro-Long® Diamond antifade mountant with DAPI (P36966, ThermoFisher

Scientific) and images captured using a Nikon A1 confocal microscope system and *NIS-*

elements software (Nikon).

Cell counts and tracing. Excluding images from thick sections, all other images

were taken on Leica CTR 5000 microscope and superimposed in Adobe Photoshop.

Electrophysiology

Cortical area of interest. For *in vitro* recording of cortical nNOS/NK1R neurons,

we targeted cells in layer V-VI at the border of the cingulum between motor cortex 1 and

cingulate cortex 2 (Bregma: 0.74mm – 0.26mm) (Franklin and Paxinos 2008). This

region of interest is readily identifiable across slices, has been previously studied

(Williams et al. 2017), and has a relatively dense expression of cortical nNOS/NK1R cells.

  In vitro recording procedures. Coronal brain slices (250 µm) were prepared in ice-cold, oxygenated (95% O_2, 5% CO_2) sucrose-based artificial cerebral spinal fluid (aCSF) containing (in mM): 250 sucrose, 2.5 KCl, 1.24 NaH_2PO_4, 10 $MgCl_2$, 10 glucose, 26 $NaHCO_3$, 0.5 $CaCl_2$ (305 mOsm/L). Slices were incubated in aCSF containing (in mM): 124 NaCl, 2.5 KCl, 1.24 NaH_2PO_4, 1.3 $MgCl_2$, 10 glucose, 26 $NaHCO_3$, 2.5 $CaCl_2$ (300 mOsm/L) at 37°C for 15 min. Thereafter, slices were maintained and recorded at 22°C with aCSF flow rate of ~1 ml/min.

  For voltage- and current-clamp recordings, the pipette solution contained (in mM): 130 K-gluconate, 2 KCl, 3 $MgCl_2$, 2 MgATP, 0.2 Na_2GTP, 10 HEPES, 0.2 EGTA (290 mOsm/L, pH 7.3). For neurons collected for scRT-PCR, 0.3% biocytin was included in the pipette solution to facilitate *post hoc* identification of patched cells. All recordings were acquired with a MultiClamp 700A amplifier, Digidata 1322A digitizer interface and pClamp 9 software (Molecular Devices). Voltage clamp data were sampled at 7kHz and filtered at 3kHZ; current clamp data were sampled at 20-25kHz and filtered at 10kHz. Changes in input resistance (R_{in}) were monitored across the experiments by injecting hyperpolarizing steps (-20pA or -40pA) periodically by switching from voltage-clamp mode and recording in current-clamp mode. Voltage-clamp recordings were then concatenated to remove breaks. For current-clamp recordings, nNOS neurons were recorded at their resting membrane potential (RMP). For voltage-clamp recordings, V_h was -60mV. We measured spontaneous excitatory postsynaptic currents (sEPSCs) in the absence of tetrodotoxin (TTX) in the circulating

11

aCSF. To measure miniature excitatory postsynaptic currents (mEPSCs), TTX (1 µM)

was added to block action potential-mediated effects for at least 8 min before the start

of a baseline period. Series resistance varied from 10-60 MΩ and was monitored during

voltage clamp recordings. Any neurons deviating >10% in series resistance over time

were excluded from analysis; the bridge balance was maintained and monitored during

current-clamp recordings. Membrane potential measurements were not corrected for

the theoretical liquid junction potential of -15mV between pipette solution and bath

solution. The reference electrode was a Ag/AgCl⁻ pellet.

Recordings of cortical nNOS/NK1R neurons from WT and ox-tTA mice. Layer V-

VI nNOS/NK1R neurons were identified in cortical slices from WT and *ox-tTA* mice

following a brief bath application of the NK1R ligand, Substance P-conjugated

tetramethylrhodamine (SP-TMR, 50nM). Previous studies have established this

approach to be highly selective for Type 1 nNOS/NK1R neurons (Dittrich et al. 2012;

Williams et al. 2017). Following a 20 min washout period, internalization of receptor-

bound fluorescent ligand enabled visualization of nNOS/NK1R cells for patch clamp

recording as described previously (Dittrich et al. 2012; Williams et al. 2017). Juvenile

mice (male and female, P13-28) were used.

Recordings of Hcrt neurons expressing ChR2 from ox-tTA mice. Neurons

expressing ChR2 were identified by expression of eYFP. Electrical fingerprints of

neurons were monitored (Williams et al. 2008) to identify likely Hcrt-expressing neurons.

Current-clamp and voltage-clamp recordings were used to assess the sensitivity of

ChR2 to blue-light duration and intensity. Single or repetitive (1Hz) 1 ms, 2 ms and 10

ms pulse widths were tested. ChR2-expressing neurons, axons, and terminals were

activated by full-field 470nm light pulses via a blue light-emitting diode (Lumencor Spectra light engine, Lumencor). This light source was coupled to the epifluorescence light path of an upright Leica DM LFSA microscope (Leica Microsystems, Germany). When light was applied through a 40x objective, a 1 mm wide beam with ~10 mW/mm^2 power density was produced that had minimal tissue heating effects as we previously reported (Williams et al. 2014).

 Recordings of cortical nNOS neurons from ox-tTA;nNOS-CreER;Ai14 mice and photostimulation of LHA afferents. Cortical nNOS neurons in adult *nNOS-CreER;Ai14 mice* were identified on the basis of their anatomical location and expression of the fluorescent tdTomato marker. For current-clamp recordings, nNOS neurons were recorded at their resting membrane potential (RMP) and any deviations in membrane potential (V_m) due to photostimulation determined. For voltage-clamp recordings, V_h was -60mV and the current evoked was recorded. Photostimulation effects on spontaneous excitatory postsynaptic currents ($sEPSC_o$) and miniature excitatory postsynaptic currents ($mEPSC_o$) were measured. The photostimulation protocol applied to activate ChR2 in LHA terminals was a 10 ms pulse at 1Hz, repeated for 30 sweeps. Application of HCRTR1 (SB-334867, 10 nM; SB) and HCRTR2 (TCS OX2 29, 10 nM; TCS) antagonists were then tested to assess a possible Hcrt receptor-mediated component.

 Recordings of nNOS/NK1R cells in juvenile mice subjected to sleep deprivation. To determine whether prolonged wakefulness affected the response of cortical nNOS/NK1R neurons to hypocretin 1 (HCRT1) application (see Results), two juvenile

WT mice (female, P17-18) were sleep deprived from ZT0 for 4 h as previously

described (Williams et al., 2017) before being sacrificed for *in vitro* electrophysiology.

    EEG/EMG recordings. Male DTA mice (> 10 weeks of age) and monogenic *ox-*

tTA controls were prepared for implantation of biotelemetry transmitters (F20-EET; Data

Sciences International, St. Paul, MN) for chronic recording of EEG, EMG, core body

temperature (T_b) and gross motor activity as previously described (Black et al. 2013;

Black et al. 2014). A sterile transmitter was placed intraperitoneally along the midline in

each mouse and the two biopotential leads routed subcutaneously to the head. EMG

leads were tethered bilaterally through the nuchal muscles. The cranial holes for EEG

leads were located at 1 mm anterior to bregma and 1 mm lateral to midline, and,

contralaterally, 2 mm posterior to bregma and 2 mm lateral to midline. Following a

period of recovery, mice were then DOX(-) for 22 weeks to ensure full degeneration of

Hcrt neurons and were housed with access to running wheels. These mice

subsequently underwent the sleep deprivation procedures described below.

Cytoplasm harvest and single-cell reverse transcription/polymerase chain

reaction (scRT-PCR)

    At the end of whole-cell recordings (<20 min duration) to record the biophysical

properties of cells in WT mice, the cytoplasmic content of SP-TMR-identified

nNOS/NK1R cells was aspirated into the recording pipette. The content of the pipette

was expelled into a test tube and RT was performed in a final volume of 10 µl as

described previously (Lambolez et al. 1992). The scRT-PCR protocol was designed to

probe simultaneously for the expression of the two Hcrt receptor mRNAs (*Hcrtr1* and

Hcrtr2) and mRNAs encoding well-established markers of cortical Type I NOS interneurons (Ascoli et al. 2008; Karagiannis et al. 2009; Dittrich et al. 2012). Neuronal markers included the vesicular Glutamate Transporter 1, the two isoforms of Glutamic Acid Decarboxylase (GAD65 and GAD67), Somatostatin (SOM), Neuropeptide Y (NPY), the neuronal isoform of Nitric Oxide Synthase (nNOS) and the substance P receptor (NK1R). A two-step amplification was performed essentially as described (Cauli et al. 1997; Cabezas et al. 2013) using the primer pairs listed in Table 1. All primer pairs were designed to span introns; 10 µl of each individual PCR product were run on a 2% agarose gel stained with ethidium bromide using ΦX174 digested by *Hae*III as a molecular weight marker. The RT-PCR protocol was tested on 1 ng of total RNA purified from mouse whole brain. All amplicons detected were the sizes predicted from published sequences (Table 2).

Sleep deprivation of mice

For experiments related to sleep homeostasis, the reference point used was lights-on or ZT (Zeitgeber Time) 0, when sleep pressure is high. DTA mice and littermate controls were subjected to one of the following experimental groups: 1) 4 h sleep deprivation (SD) or 2) 4 h SD followed by 2 h recovery sleep (RS). SD was initiated at lights on (ZT0; 9:00am) and consisted of progressive stimulation (i.e., removal of cage lid at the beginning of the session, followed by light cage tapping or presentation of toys in the middle and, if required, gentle stroking of vibrissae with a brush towards the end of the SD period) in the home cage to keep mice awake for the 4 h duration. Mice in the recovery sleep (RS) group were undisturbed for 2 h after the 4 h

SD period. At the end of the SD or RS period, mice were deeply anesthetized (see below), perfused transcardially and the brain removed for histological processing.

Chemicals

Hypocretin1 (HCRT1; hypocretin1 peptide, 100nM), SB-334867 (SB; HCRTR1 antagonist, 10nM), TCS OX2 29 (TCS; HCRTR2 antagonist, 10nM), bicuculline methobromide (BIC; $GABA_AR$ antagonist, 10 µM), 2-hydroxysaclofen (2-HS; $GABA_BR$ antagonist, 5 µM), DL-AP5 (AP-5; NMDAR antagonist, 100 µM), and CNQX disodium salt (CNQX; AMPA/KA receptor antagonist, 7 µM) were from Tocris. Tetrodotoxin (TTX; 1 µM) was from abcam. All other chemicals were from Sigma-Aldrich.

Data analyses and statistics

In vitro electrophysiology. Patch-clamp recording data were analyzed using Clampfit 9 (Molecular Devices) and synaptic events using MiniAnalysis (Synaptosoft). The nonparametric Kolmogorov–Smirnov test (K-S test; MiniAnalysis) was used to quantify the effects of bath applied pharmacological treatments (5 to 10 min post HCRT1 application to encapsulate peak effect, unless otherwise stated) or photostimulation on sEPSC and mEPSC frequency for each group. For EPSC ANOVA analysis, peak effects were measured at 6 to 9 min post HCRT1 application unless otherwise stated. Sample traces were generated with Igor Pro v6 (WaveMetrics) and graphs produced with Prism 5 (GraphPad). For other cells, V_m was taken in 30 s bins for a minimum period of 4 min prior to intervention. These data were then used to calculate the average baseline V_m or resting membrane potential (RMP). The effects of

interventions on V_m were compared to this average baseline and the delta calculated. For voltage-clamp analyses, cells were included if the peak current was greater than the mean ± 2*SD of the preceding baseline value. The baseline for all cells tested was -2.04 ± 6.74 pA (mean ± SD). To assess characteristics of glutamatergic events between genotypes, 200 events per baseline period were taken for analysis. Unless otherwise stated, data are presented as mean ± SEM with n = number of cells per group (represented in parenthesis for Figures). We compared group means from the same cells using paired t-tests or one-way ANOVA followed by Newman-Keuls *post hoc* tests; changes over time were analyzed by repeated measures (RM)-ANOVA or two-way ANOVA followed by the Bonferroni or Newman-Keuls *post hoc* test; different groups of cells were then compared using unpaired t-tests. For EEG parameters, two-way ANOVA with Bonferroni *post hoc* tests were performed. A statistical significance threshold of $P < 0.05$ was used.

Sleep/wake recordings. EEG data from DTA mice and monogenic *ox-tTA* controls were scored in 10 s epochs by experts (≥ 96% inter-rater reliability) using NeuroScore 2.1 (Data Sciences). Epochs were classified as wakefulness (mixed-frequency, low-amplitude EEG and high-amplitude, variable EMG); wakefulness with wheel-running, REM sleep (theta-dominated EEG and EMG atonia); NREM sleep (low-frequency, high-amplitude EEG and low-amplitude, steady EMG); or cataplexy. Criteria for cataplexy were ≥10 s of EMG atonia, theta-dominated EEG, and video-confirmed behavioral immobility preceded by ≥40 s of W (Scammell et al. 2009). Data were analyzed as time spent in each scored classification per category (SD or RS). For the RS group, the final 90 min period of the 2 h sleep opportunity period was scored. To

assess sleep intensity, EEG spectra during NREM sleep were computed using the fast

Fourier transform algorithm in NeuroScore (Data Sciences) on all 10 s epochs without

visually detectable artifact. EEG delta power (0.5–4 Hz) in NREM sleep (NRD) was

calculated. NRD power was then multiplied by the time (h) spent in NREM sleep to

calculate NRD energy (NRDE). Results were tested for significance by two-way ANOVA

with genotype and "sleep condition" (SD, RS) as factors. When ANOVA indicated

significance, contrasts between relevant factor levels were detected with *post hoc*

Bonferroni *t* tests with α = 0.05.

Results

Cortical nNOS/NK1R neurons are excited by hypocretin 1 in the mouse

Previous studies (Hay et al. 2015; Wenger Combremont et al. 2016a, 2016b)

have shown that neurons located in deep cortical layers were responsive to bath

application of either hypocretin 1 or hypocretin 2 (also known as orexin-A and orexin-B,

respectively). Therefore, we investigated whether cortical nNOS/NK1R neurons were

also responsive (Fig. 1Ai). We identified nNOS/NK1R neurons in layers V-VI of the

cingulate cortex using the fluorescent NK1R ligand SP-TMR (50 nM) (Fig. 1A ii-iii). Bath

application of hypocretin 1 (HCRT1, 100 nM) predominantly evoked an inward current in

voltage-clamp recordings (-12.87 ± 2.39 pA, *n* = 10 of 15; paired *t*-test, $t_{(9)}$ = 5.16, *P* =

0.0006; Fig. 1B and 1H). This coincided with a membrane (V_m) depolarization in

current-clamp (BL: -64.75 ± 1.44 mV vs. HCRT1: -60.71 ± 1.92 mV, paired *t*-test, $t_{(8)}$ =

3.96, *P* = 0.004; Fig. 1C and 1I) and a small but non-significant increase in firing rate

(BL: 9.69 ± 1.67 Hz vs. HCRT1: 12.59 ± 0.82 Hz n = 5; one-way ANOVA, $F_{(2,14)}$ = 2.49, P = 0.14). The remaining cells in both recording modes did not show any significant change in current or membrane potential responses to HCRT1 application relative to baseline.

Since multiple cell types in the cortex show sensitivity to application of hypocretin peptides (Lambe and Aghajanian 2003; Bayer et al. 2004; Hay et al. 2015; Wenger Combremont et al. 2016a), there may be indirect influences on cortical nNOS/NK1R activity. Therefore, we applied HCRT1 in the presence of the Na^+-channel blocker tetrodotoxin (TTX; 1µM) to block HCRT1-mediated action-potential dependent effects. As indicated in Fig. 1D, HCRT1 also evoked an inward current in TTX (Δ-7.96 ± 0.92 pA; n = 17 of 19; paired t-test, $t_{(16)}$ = 8.72, $P < 0$.0001) as well as V_m depolarization (Δ+3.54 ± 0.46 mV, n = 9 of 14; Fig. 1E and 1I), neither of which were significantly different from HCRT1 responses in normal aCSF (I: one-way ANOVA, $F_{(2,32)}$ = 0.90, P = 0.41; V_m: one-way ANOVA, $F_{(2,21)}$ = 0.74, P = 0.48). Changes in input resistance under TTX indicated a closure of channels with HCRT1 application in most cells (BL: 333.1 ± 27.55 MΩ vs. HCRT1: 356.6 ± 26.75 MΩ, n = 5; one-way ANOVA, $F_{(2,14)}$ = 7.46, P = 0.01). To confirm a true postsynaptic response, we applied HCRT1 in 0 Ca^{2+}/ 3.3 Mg^{2+} aCSF containing TTX, blockers for both glutamate (CNQX, 7µM and AP-5, 100 µM) and GABA (BIC, 10µM and 2-HS, 5 µM) (Fig. 1F and 1G). Under these conditions, significant excitation responses remained (Δ-7.44 ± 0.75 pA; n = 6 of 7, and Δ+2.27 ± 0.39 mV; n = 4 of 6; Fig. 1H and 1I).

Previously, we found that the effects of the cholinomimetic carbachol on nNOS/NK1R excitability were largely unchanged with sleep deprivation (Williams et al.

2017). Therefore, we were interested to determine whether or not responses to HCRT1 were affected by a similar challenge to the sleep homeostatic system. We assessed whether HCRT1 could evoke a response on cortical nNOS/NK1R neurons in brain tissue taken from mice previously subjected to 4 h sleep deprivation (4 h SD). In 4 h SD mice, HCRT1-evoked current and membrane depolarization responses in TTX were not significantly different from baseline (BL: -63.99 ± 5.71 mV vs. HCRT1: -62.45 ± 6.43 mV, paired t-test, $t_{(2)}$ = 2.06, P = 0.18; and BL: -3.13 ± 0.29 pA vs. HCRT1: -4.27 ± 0.59 pA, paired t-test, $t_{(2)}$ = 1.92, P = 0.19). This contrasts significantly from the HCRT-1 mediated responses obtained in undisturbed mice (Fig. 1H; one-way ANOVA, $F_{(2,32)}$ = 4.39, P = 0.02; I: Δ -1.14 ± 0.59 pA; n = 3, unpaired t-test, $t_{(18)}$ = 2.90, P = 0.009; and $V_{m:}$ Δ+1.34 ± 0.65 mV; n = 3, unpaired t-test, $t_{(10)}$ = 2.49, P = 0.03; Fig. 1H-I). These results demonstrate that HCRT1 directly affects cortical nNOS/NK1R neurons and that the response of these cells to HCRT1 is dependent on prior sleep/wake history.

Hypocretin 1 affects cortical nNOS/NK1R neurons predominantly via HCRTR1

HCRTR1 and HCRTR2 are G protein-coupled receptors that mediate the main effects of HCRT1; both receptors have been localized in the mouse cerebral cortex (Mishima et al. 2008). Therefore, we used antagonists for both receptors, SB-334867 (SB; HCRTR1 antagonist, 10 nM) and TCS OX2 29 (TCS; HCRTR2 antagonist, 10 nM; Fig. 2A), to investigate the mode of HCRT1 action on cortical nNOS/NK1R neurons.

As indicated in Fig. 2A and 2B, HCRTR antagonists had significant effects on responses to HCRT1 in both voltage clamp (one-way ANOVA, $F_{(3,26)}$ = 9.34, P = 0.0003) and current-clamp (one-way ANOVA, $F_{(3,24)}$ = 13.63, $P < 0.0001$). Application of SB in

TTX significantly reduced the HCRT1-mediated inward current by 63% (Δ -2.88 ± 1.01

pA; n = 5, one-way ANOVA with Newman-Keuls *post hoc* test, P < 0.05). V_m

depolarization was significantly reduced by 76% (Δ +0.75 ± 0.33 mV; n = 4, one-way

ANOVA with Newman-Keuls *post hoc* test, P < 0.001). In comparison, pre-application

of TCS had no effect on HCRT1-induced current (Δ -5.88 ± 1.00 pA, n = 4; one-way

ANOVA with Newman-Keuls *post hoc* test, P > 0.05) or V_m (Δ +3.15 ± 0.51 mV; n = 4,

one-way ANOVA with Newman-Keuls *post hoc* test, P > 0.05). In the presence of both

antagonists (+SB/TCS) HCRT1-mediated current and V_m were blocked (I: Δ -0.25 ± 0.92

pA; n = 9, one-way ANOVA with Newman-Keuls *post hoc* test, P < 0.001; V_m: Δ +0.01 ±

0.49 mV; n = 8, one-way ANOVA with Newman-Keuls *post hoc* test, P < 0.001). These

results indicate that HCRT1 primarily affects cortical nNOS/NK1R neurons via HCRTR1.

A role for HCRTR1 signalling in cortical nNOS/NK1R neurons of the cingulate

cortex

Immunohistochemical analysis of brain tissue from *Hcrtr1-EGFP* mice

documented that deep layer cortical nNOS neurons colocalized with GFP

immunoreactivity, largely limited to cingulate cortical cells (Fig. 2C). Notably, there were

significantly greater proportions of other cells in this region expressing GFP

immunoreactivity signal close to cortical nNOS cells. To further identify whether

HCRTR1 was expressed in cortical nNOS/NK1R neurons, we performed single-cell

reverse transcription polymerase chain reaction (scRT-PCR) on the cytoplasmic

contents of SP-TMR identified cortical nNOS/NK1R neurons (Fig. 2D). Of 13 cortical

nNOS/NK1R cells collected, 4 cells (31%) expressed *Hcrtr1* mRNA. This proportion is

consistent with other observations that less than half of cortical neurons expressing both

Nos1 and *Tacr1* mRNA also express Hcrtr1 mRNA (Tasic et al. 2016; Paul et al. 2017).

These data suggest that cortical nNOS/NK1R cells mediate HCRTR1 effects in the

cingulate cortex, yet form a minor subset of other HCRTR1-expressing neurons.

HCRT1-mediated regulation of glutamatergic input to cortical nNOS/NK1 cells

Following application of HCRT1, some cortical nNOS/NK1R cells underwent a

burst-like increase in EPSCs. Therefore, we assessed whether HCRT1 had any effects

on glutamatergic tone (Fig. 3). We found that a main effect of HCRT1 application was a

reduction in sEPSC activity (80.85 ± 1.93%, RM-ANOVA, $F_{(2,20)}$ = 12.49, P = 0.001; n =

6; Fig. 3A; K-S test = 0.02). In TTX (1 µM), HCRT1 did not have a discernible effect on

mEPSC activity compared to baseline at the time point measured (6 to 9 min post

application; 104.3 ± 1.33%, n = 14; RM-ANOVA, $F_{(2,20)}$ = 0.59, P = 0.57; Fig. 3B; K-S

test = 0.09).

Since we did not find a consistent effect of HCRT1 on glutamatergic input, the

burst-like increase in EPSCs could be due to variations in presynaptic HCRTR

distribution on glutamatergic terminals. Therefore, we examined the effect of HCRTR1

and HCRTR2 antagonists on mEPSC activity. In the presence of SB-334867 (+SB; 10

nM), HCRT1 increased mEPSC frequency (131.1 ± 4.75%, n = 5; RM-ANOVA, $F_{(2,20)}$ =

13.34, P = 0.0027; Fig. 3C; K-S test = 0.0002) relative to baseline (BL -4 to -1min: 110.0

± 3.35%, n = 5). In the presence of TCS OX2 29 (TCS; 10 nM), HCRT1 also increased

the frequency of mEPSCs (BL: 97.12 ± 3.21% and +TCS: 121.6 ± 6.34%, n = 3; RM-

ANOVA, $F_{(2,20)}$ = 7.93, P = 0.006; Fig. 3D; K-S test = 0.001) but the time course of the

increase was delayed relative to blockade by SB-334867. When both antagonists were

pre-applied, HCRT1 did not significantly change mEPSC frequency (BL: 99.05 ± 1.47%

vs. +SB/TCS: 105.5 ± 4.64%, n = 7; RM-ANOVA, $F_{(2,20)}$ = 1.43, P = 0.28; Fig. 3E; K-S

test = 0.25).

There was no significant effect of HCRT1 application on the amplitude of

sEPSCs ($mean_{BL}$: 7.55 ± 0.05 pA and $mean_{HCRT1}$: 7.68 ± 0.09 pA; K-S test: 0.53) or

mEPSCs ($mean_{BL}$: 8.84 ± 0.09 pA and $mean_{HCRT1}$: 8.92 ± 0.32 pA; K-S test = 0.53).

Nor was there an effect of the HCRTR antagonists on mEPSC amplitude at the time

where the peak change in frequency was recorded (+SB: $mean_{BL}$: 8.08 ± 0.42 pA and

$mean_{HCRT1}$: 8.17 ± 0.29 pA; K-S test = 0.25; +TCS: $mean_{BL}$: 10.09 ± 0.11 pA and

$mean_{HCRT1}$: 10.22 ± 0.21 pA; K-S test = 0.99; +SB/TCS: $mean_{BL}$: 8.22 ± 0.11 pA and

$mean_{HCRT1}$: 8.13 ± 0.08 pA; K-S test = 0.87). Overall, these data suggest that both

HCRTR1 and HCRTR2 negatively modulate glutamatergic tone onto cortical nNOS/NK1

neurons.

Expression of channelrhodopsin-2 in Hcrt neurons

To evaluate the functionality of the hypocretinergic effect on cingulate cortex

nNOS/NK1R neurons, we bilaterally injected AAV(DJ)-TetO-ChR2(ET/TC)-eYFP (200nl

per side) into the tuberal hypothalamus of *ox-tTA*;*nNOS-CreER;Ai14* mice (Fig. 4Ai)

followed by tamoxifen injection (75 mg/kg, *i.p*.) 3 weeks later. As indicated above, the

vast majority of transfected cells were in the LHA so, for simplicity, we refer below to the

transfected cells as from the LHA. In *ox-tTA*;*nNOS-CreER:Ai14* mice, we

optogenetically stimulated the ChR2-expressing LHA neurons to assess temporal

sensitivity of the ChR2 to blue-light (470 nm) application (Fig. 4B). In voltage-clamp, a 2 ms pulse width (1 Hz for 30 s) application of blue light at different LED power intensities indicated that the greatest change in I_o occurred between 2- 5% LED power intensities, whereas >5% power approached I_o saturation levels (I_o; RM-ANOVA with Newman-Keuls, $F_{(5,25)}$ = 41.65, P < 0.0001). For current-clamp, the same protocol revealed significant differences in light-evoked membrane depolarization (Vm_o). At LED power intensities <5%, each step-increment in power significantly increased Vm_o while changes in Vm_o approached saturation at LED power intensities >5% (RM-ANOVA with Newman-Keuls, $F_{(5,25)}$ = 29.64, P < 0.0001; Fig. 4Bi), suggesting a saturation effect or membrane depolarization block. We also tested a 10 ms pulse width (1 Hz for 30 s; Fig. 4Bii) and found that it evoked significantly greater current (Δ -634 ± 98.58 pA) than a 2 ms pulse (Δ -219 ± 67.72 pA) at the same intensity (2%; paired t-test, $t_{(5)}$ = 3.91, P = 0.01). In comparison, no significance difference occurred in Vm_o (10 ms: Δ +36.6 ± 8.67 mV vs. 2ms: Δ +25.1 ± 6.58 mV; paired t-test, $t_{(3)}$ = 1.19, P = 0.32). Action potentials (single or multiple) concurrent with blue-light stimulation were evoked in 3 of 4 ChR2-expressing cells, with a mean decay time of 23.5 ± 5.45 ms. These data indicate successful expression of ChR2 in neurons of the LHA.

For histological verification, we bilaterally injected the same AAV(DJ)-TetO-ChR2(ET/TC)-eYFP into the LHA of *ox-tTA* and WT mice and, after a 4 week *in vivo* incubation period, confirmed ChR2 expression in Hcrt neurons (Fig. 4C) of the LHA. The transduction efficiency of ChR2 to Hcrt neurons was significantly greater in the *ox-tTA* mice compared to WT mice (60.3 ± 10.7% and 26.2 ± 8.0%, respectively; P = 0.04). The specificity of ChR2 to Hcrt neurons was 79.7 ± 3.0% in *ox-tTA* mice. In both

genotypes, the number of Hcrt neurons counted for analysis was comparable (*ox-tTA:* 83.2 ± 9.70 and WT: 99.7 ± 11.17). These data indicate that viral expression of ChR2 is primarily directed to Hcrt-containing neurons but that the viral construct is not completely dependent upon a functional *tTA-TetO* system since ChR2 expression occurred, to some extent, in WT mice. Nonetheless, ChR2 expression in the Hcrt field of *ox-tTA* mice is comparable to that of other AAVs used in different mouse models (Sasaki et al. 2011).

Next, we assessed whether we could photoevoke responses in cortical nNOS/NK1R neurons by terminal stimulation of LHA afferents. These experiments were performed after bilateral injection of ChR2 into the LHA of *ox-tTA;nNOS-CreER:Ai14* mice (Fig. 4Di), which resulted in ChR2 projection fibers in the cingulate cortex (Fig. 4Dii). Since there were no Hcrt cell bodies in our slice preparations of the cingulate cortex, we utilized a photostimulation protocol of 10 ms pulse width at 100% LED power (1 Hz for 30 s) to promote depolarization of terminals in the absence of cell-body driven terminal release of neurotransmitters (Fig. 5A). This protocol was chosen based on the finding that a 10 ms light pulse of ChR2-cell bodies in the LHA evoked considerably greater current in LHA neurons than the 2 ms pulse width and, therefore, should ensure maximal photostimulation of the distant terminals in slices lacking the LHA ChR2 cell bodies. Similar illumination levels have previously been employed in studies of corticopedal projections (Hay et al. 2015; Williams et al. 2017). Examples of voltage-clamp recordings from cortical nNOS/NK1R cells before and after photostimulation of terminal Hcrt-containing LHA afferents are shown in Fig. 5Aiii and Fig. 5Aiv shows 20 s recordings of EPSC activity. Among the nNOS/NK1R cells

analyzed, only 3 of 10 cells tested had significant inward currents to blue-light stimulation (ΔI_o: -6.68 ± 0.29 pA; paired t-test, $t_{(2)}$ = 6.05, P = 0.03; responses denoted in black in Fig. 5Av). When photostimulation was repeated in the presence of TTX (1 µM) and 4-aminopyridine (4-AP; 0.5 µM), only 2 of 7 cells had significant inward currents (ΔI_o: -4.63 ± 0.10 pA). When photostimulation was repeated with the pre-application of HCRTR antagonists (+SB/TCS), no cells tested had measureable I_o (BL: -2.34 ± 0.10 pA and I_o: -2.67 ± 0.57 pA, n= 7; paired t-test, $t_{(6)}$ = 0.88, P = 0.41), including the two cells that had previously exhibited a detectable current.

We next analyzed the effect of photostimulation on glutamatergic tone onto cortical nNOS/NK1R cells as, on occasion, there were noticeable changes in EPSC activity during the course of recording (Fig. 5Aiv). Blue-light stimulation evoked time-locked sEPSC activity in 4 of 13 cortical nNOS/NK1R cells (Fig. 5B). In addition, sEPSC frequency (BL: 1.3 ± 0.03 Hz) significantly increased following photostimulation ~6 min post-stimulation (127.3 ± 3.38%; n = 13, RM-ANOVA with Newman-Keuls *post hoc* test, $F_{(2,10)}$ = 10.16, P = 0.004; K-S test < 0.00001). In comparison to sEPSC activity, there were no cells recorded in the presence of TTX and 4-AP that demonstrated discernible time-locked mEPSC activity (Fig. 5C). Nevertheless, the frequency of mEPSC activity increased significantly after photostimulation (127.3 ± 3.38%; n = 7, RM-ANOVA with Newman-Keuls *post hoc* test, $F_{(2,10)}$ = 2.65, P = 0.0009; K-S test = 0.002). Pre-application of HCRTR antagonists SB-334867 and TCS OX2 29 (+SB/TCS; Fig. 5D) blocked the increase in mEPSC frequency seen with blue-light stimulation of LHA afferents (99.66 ± 4.62%; n = 7, RM-ANOVA with Newman-Keuls *post hoc* test, $F_{(2,10)}$ = 0.37, P = 0.7; Fig. 3F; K-S test = 0.73). There was no effect of

photostimulation on sEPSC amplitude (BL: 8.78 ± 0.11 pA; K-S test = 0.54), mEPSC

amplitude (BL: 7.17 ± 0.09 pA; K-S test = 0.03), or in the presence of HCRTR

antagonists (BL: 7.49 ± 0.15 pA; K-S test: 0.99). Together, these results demonstrate

that stimulation of LHA afferents to the cingulate cortex, likely from Hcrt neurons,

predominately increased presynaptic glutamatergic input onto cortical nNOS/NK1R

neurons, with a small minority (28%) of nNOS/NK1R cells demonstrating a hcrt-

mediated postsynaptic current.

Hcrt neuron degeneration affects cortical nNOS/NK1R neurons

To evaluate the functionality of Hcrt innervation of cingulate cortex nNOS/NK1R

neurons, we assessed the electrical properties of these neurons in *ox-tTA;TetO-DTA*

mice in which Hcrt neuron degeneration can be induced. Male and female breeders

were paired and taken off chow containing doxycycline (DOX(-)), facilitating the

expression of diptheria toxin fragment A (DTA) leading to Hcrt cell loss (Tabuchi et al.

2014). The resultant *ox/tTA;TetO-DTA* offspring (DTA[+]; male and female, P21 and P28)

were taken for *ex vivo* electrophysiology (Fig. 6Ai) or histology (Fig. 6Aii; *n* = 4). To

verify Hcrt cell loss, mice whose parents remained on DOX for conception and weaning

(DOX(+); *n* = 3) were used as controls and age-matched to examine histological

differences. DOX(-) pups had significantly fewer Hcrt cells than DOX(+) pups (20.3 ±

4.0 vs. 97.8 ± 25.9 cells, $t_{(5)}$ = 3.50, *P* = 0.02), controlled for anatomical location. This

significant reduction of the number of Hcrt cells was accompanied by a clear difference

in Hcrt staining intensity between the two groups (Fig. 6Aii).

To determine whether this reduction in the number of Hcrt neurons and thus Hcrt afferents to the cortex affected the properties of cortical nNOS/NK1R neurons, we compared the RMP and resistance of cortical nNOS/NK1R cells between DOX(-) DTA and WT mice (P21-28). Although there was no difference between genotypes in RMP (WT: -52.7 ± 2.70 mV, n = 11 vs. DTA: -51.3 ± 2.78 mV, n = 13; unpaired t-test, $t_{(22)}$ = 0.37, P = 0.72), input resistance was significantly higher in DOX(-) DTA mice (WT: 411.6 ± 50.94 MΩ, n = 10 vs. DTA: 820.7 ± 135.5 MΩ, n = 11; unpaired t-test, $t_{(19)}$ = 2.72, P = 0.01).

Analysis of glutamatergic input onto cortical nNOS/NK1R neurons also revealed differences between genotypes. Although the sEPSC frequency did not differ (WT: 2.51 ± 0.84 Hz, n = 11 vs. DTA: 1.54 ± 0.36 Hz, n = 9; unpaired t-test, $t_{(18)}$ = 0.97, P = 0.34), the mean sEPSC amplitude was greater in DTA mice (WT: 7.76 ± 0.08 pA, n = 11, vs. DTA: 8.56 ± 0.09 pA, n = 9; unpaired t-test, $t_{(398)}$ = 6.55, P < 0.0001; Fig. 6B). The frequency of mEPSCs was significantly reduced in DOX(-) DTA mice (WT: 2.01 ± 0.29 Hz, n = 12 vs. DTA: 1.12 ± 0.18 Hz, n = 7; unpaired t-test, $t_{(17)}$ = 2.12, P = 0.04) and the mean mEPSC amplitude was also greater (WT: 7.18 ± 0.06 pA, n = 12 vs. DTA: 7.57 ± 0.09, n = 7; unpaired t-test, $t_{(398)}$ = 3.25, P = 0.001; Fig. 6C). Within genotype comparisons revealed that TTX significantly reduced the amplitude of events (WT: unpaired t-test, $t_{(399)}$ = 3.32, P = 0.0001; DTA: unpaired t-test, $t_{(399)}$ = 3.68, P = 0.0003) but not event frequency (WT: unpaired t-test, $t_{(21)}$ = 0.57, P = 0.57; DTA: unpaired t-test, $t_{(14)}$ = 0.96, P = 0.35). These data indicate that a chronic loss of Hcrt input can affect glutamatergic input to cortical nNOS/NK1R cells.

Reduction of Hcrt afferents to the cortex via Hcrt cell body degeneration in DOX(-) DTA mice may affect the sensitivity of the response by cortical nNOS/NK1R neurons to Hcrt release. Therefore, we bath applied HCRT1 to investigate if any changes occurred. In voltage-clamp, only 2 of 7 cortical nNOS/NK1R neurons had discernible currents (Δ -4.14 ± 0.55 pA; Fig. 6D) and, in TTX (1µM), the proportion of responders was 1 in 5 (Δ -5.83 pA; Fig. 6E). When we analyzed sEPSC activity, HCRT1 significantly reduced glutamatergic input (80.31 ± 5.27% at 8-11 min post-application relative to baseline; n = 4, RM-ANOVA, $F_{(2,12)}$ = 5.40, P = 0.020; Fig. 4E; K-S test = 0.0004). HCRT1 also significantly reduced the amplitude of events onto cortical nNOS/NK1R cells to 8.23 ± 0.2 pA (88.79 ± 1.81% at 8-11 min post-application relative to baseline; n = 4, RM-ANOVA, $F_{(2,12)}$ = 11.49, P = 0.002; K-S test = 0.001; Fig. 6Diii). In comparison, we found no change in mEPSC frequency following HCRT1 application (101.6 ± 9.33% at 8-11 min post-application relative to baseline; n = 4, RM-ANOVA, $F_{(2,12)}$ = 1.67, P = 0.38; K-S test = 0.26; Fig. 6Eiii) and no significant change in event amplitude (9.93 ± 0.15pA) compared to baseline (103.0 ± 1.68% at 8-11 min post-application relative to baseline; n = 4, RM-ANOVA, $F_{(2,12)}$ = 3.03, P = 0.08; K-S test = 0.87). Membrane resistance changes indicated that a closure of membrane channels likely occurred following HCRT1 application (BL: 433.6 ± 157.3 MΩ vs. HCRT1: 496.9 ± 183.1 MΩ; n = 4; RM-ANOVA, $F_{(2,11)}$ = 4.86, P = 0.055). These data indicate that a chronic loss of Hcrt input can also affect the sensitivity of the response by cortical nNOS/NK1R neurons to Hcrt release.

Hcrt neuron degeneration does not affect sleep homeostasis or sleep-related
expression of c-FOS in cortical nNOS/NK1R neurons

Since cortical nNOS/NK1R neurons have been implicated in sleep homeostasis,
we investigated whether the loss of Hcrt input and the consequent alterations in activity
of these cells described above affected EEG slow wave activity and the previously-
reported increases in c-FOS expression within these neurons during recovery sleep.
Thus, we compared the responses of Hcrt-deficient DOX(-) DTA mice and Hcrt-intact
monogenic control (MC) mice to sleep deprivation and recovery sleep. All mice had
been off DOX for >22 weeks, well beyond the reported time required (4 weeks) for
>97% degeneration of the Hcrt neuronal field; monogenic control (MC) mice lacked the
paired tTA and TetO transgenes that permit Hcrt neurodegeneration (Tabuchi et al.,
2014). Sleep deprivation (SD) occurred at a time of day (ZT0-4) during which the
homeostatic drive to sleep is high in mice. Mice were sacrificed either immediately after
SD, or after a 2 h recovery sleep (RS) period. Immunohistochemistry was performed on
brain sections from both groups to determine the percent of cortical nNOS/NK1R
neurons that expressed c-FOS (Fig. 7A).

The percentage of time in each arousal state, the corresponding measures of
sleep intensity and the percentage of cortical nNOS/NK1R neurons that expressed c-
FOS during the 90 min prior to sacrifice for the four experimental groups are shown in
Table 3 and Fig. 7B. For all parameters except cataplexy, 2-way ANOVA revealed
significant variation with a main effect of "sleep condition" without an effect of genotype
or any genotype x condition interaction. The amount of NREM sleep lost and recovered
did not depend on genotype; thus, the SD procedure was effective and equivalent

between DTA and MC mice. Since DOX(-) DTA mice were more difficult to keep awake than the MC mice, the DTA mice exhibited enough additional epochs of NREM sleep that NREM delta power could be measured during SD. Nonetheless, during the subsequent 2 h RS period after the 4h SD, NREM delta power did not differ between genotypes. In addition, there was no effect of genotype on NREM delta energy (NRDE; Fig. 7B, left panel). An increased percentage of c-FOS$^+$/nNOS cells were observed during RS compared to SD in both genotypes but the proportion of c-FOS$^+$ nNOS neurons was comparable in these two strains (Fig. 7B, right panel). These results indicate that sleep-dependent activation of cortical nNOS/NK1R neurons is independent of Hcrt input.

Discussion

The hypocretin/orexin system is well known to be involved in maintenance of vigilance state. During spontaneous wakefulness and during sleep deprivation, c-FOS expression increases in Hcrt-containing neurons (Estabrooke et al. 2001), suggesting increased electrical activity of these cells. Hcrt-containing fibers innervate the cortex (Peyron et al. 1998; Jin et al. 2016) and Hcrt peptides are known to excite cortical neurons (Lambe and Aghajanian 2003), including deep layer neurons (Bayer et al. 2004; Hay et al. 2015; Wenger Combremont et al. 2016a, 2016b). Lastly, transcriptomic studies have provided evidence for *Hcrtr1* mRNA expression in cortical nNOS/NK1R neurons (Tasic et al. 2016; Paul et al. 2017). Consequently, we determined whether HCRT1 affects cortical nNOS/NK1R cells and whether Hcrt innervation contributes to sleep homeostasis-related activation of these cells

(Gerashchenko et al. 2008; Morairty et al. 2013). The cingulate cortex was investigated

as this region contains numerous cortical nNOS/NK1R neurons for targeting and has

been implicated as sleep-active in primates (Rolls et al. 2003) yet also plays a role in

sustaining arousal in a novel environment (Gompf et al. 2010). In addition, the cell

density of this region is reduced in patients with narcolepsy (Joo et al. 2011) and a

reduction in somatostatin expression occurs in major depressive disorder, where sleep

disturbances of both hypersomnia and insomnia are reported (Mendlewicz 2009; Tripp

et al. 2011). Therefore, an interaction between the wake-promoting Hcrt system and

sleep-active nNOS/NK1R cells in this cortical region could underlie all of these reported

findings.

Cortical nNOS/NK1R neurons are excited by HCRT1

Bath application of HCRT1 (100 nM) evoked an inward current and membrane

depolarization of cortical nNOS/NK1R neurons which was postsynaptic and

predominantly HCRT1R-mediated. This response was not seen in cortical tissue from

mice deprived of sleep for 4 h, consistent with optogenetic studies that suggest sleep

pressure reduces the effectiveness of Hcrt signaling (Carter et al. 2009). HCRT1

reduced action potential-derived synaptic release of glutamate onto cortical nNOS/NK1

neurons but appeared to have little direct effect on presynaptic terminals. When

HCRT1 was applied in the presence of TTX, blockade of HCRTR1 or HCRTR2

significantly increased EPSC frequency, while there was no effect on EPSC amplitude.

These effects suggest that presynaptic glutamatergic tone onto cortical nNOS/NK1

neurons may be negatively regulated by both receptors, possibly on different terminals

as the temporal dynamics in the recorded EPSC frequency change was different with each HCRTR antagonist.

Optogenetic targeting of Hcrt neurons and photostimulation of Hcrt terminals in the cingulate cortex supported the possibility of endogenous Hcrt signaling onto cortical nNOS/NK1R neurons. The number of cells with measurable current was lower than with HCRT1 bath application (without TTX: 30%) but consistent in TTX (~28%). Since we did not have 100% transduction efficiency of LHA Hcrt neurons and we do not know the relative proportion of Hcrt neurons that project to the cingulate cortex, a lower response rate of cortical nNOS/NK1R cells to photostimulation compared to pharmacological experiments was not unexpected. Nevertheless, we did not find any cortical nNOS/NK1R cells that responded to photostimulation in the presence of HCRTR antagonists, including cells that had previously demonstrated photo-evoked current. Photostimulation also increased glutamatergic input onto cortical nNOS/NK1R cells and HCRTR antagonists blocked this increase. The effect of increased mEPSC activity differed from the effects observed with pharmacological application of HCRT1 which may be due to selective activation of ChR2-expressing Hcrt terminals in the vicinity of cortical nNOS/NK1 neurons rather than to activation of all HCRTR-expressing terminals, as likely occurs with bath application of a compound.

scRT-PCR supports HCRTR1 as the main Hcrt postsynaptic receptor on cortical nNOS/NK1R neurons

Pharmacological application of HCRTR antagonists indicated that HCRTR1 was principally involved in the direct HCRT1 response of cortical nNOS/NK1R neurons. To

investigate this further, we analyzed cortical tissue from *Hcrtr1-EGFP* mice for co-expression with layer V-VI nNOS neurons and performed scRT-PCR. Immunohistochemical results indicated HCRTR1 expression in a subset of cingulate cortical neurons confined to layer V-VI but the expression in cortical nNOS cells was sparse. In addition, scRT-PCR indicated that 31% of nNOS cells expressed *Hcrtr1* mRNA without evidence for *Hcrtr2* mRNA expression. These results are similar to the proportion of cortical nNOS/NK1R neurons that were responsive to photostimulation of Hcrt afferents and consistent with other recent transcriptomic studies (Tasic et al. 2016; Paul et al. 2017). Together, these data support the conclusion that the effects of HCRT1 on cingulate cortex nNOS/NK1R cells are predominantly mediated by postsynaptic HCRTR1.

Hcrt neuron degeneration affects the HCRTR1-mediated response of cortical nNOS/NK1R cells but not sleep homeostasis

Degeneration of Hcrt neurons results in loss of Hcrt-containing afferents to sleep/wake regulatory sites and a profound disruption of sleep/wake architecture in mice (Hara et al. 2001; Tabuchi et al. 2014) as well as human narcoleptics (Peyron et al. 2000; Thannickal et al. 2000). Nonetheless, the homeostatic challenge posed by sleep deprivation (SD) evokes the normal increase in EEG NREM delta power and time spent in NREM in Hcrt KO mice (Mochizuki et al. 2004) and in narcoleptic patients (Tafti et al. 1992). To determine whether Hcrt neuron loss affects the c-FOS expression that occurs in cortical nNOS/NK1R neurons during rebound sleep after sleep deprivation, we utilized *ox-tTA;TetO-DTA* mice (Tabuchi et al. 2014).

Cortical nNOS/NK1R cells from juvenile DOX(-) DTA mice exhibited some differences in their biophysical properties compared to age-matched WT mice. Although these cells received glutamatergic events of greater amplitude than WT mice, the effect of HCRT1 on glutamatergic input and the magnitude of inward current evoked were comparable to WT mice. The proportion of cells responsive to HCRT1 application in voltage clamp was reduced (DTA: ~24% vs. WT: ~77%) but this percentage of cells was similar to the percentage that were responsive in the photostimulation experiments in WT mice, although lower than the proportion of cortical nNOS/NK1R cells expressing *Hcrtr1* mRNA as determined by scRT-PCR. Therefore, despite some changes in basal characteristics of cortical nNOS/NK1R cells in juvenile DTA mice, the responsiveness to exogenously applied HCRT1 seems minimally affected by loss of Hcrt innervation.

EEG recordings from adult DOX(-) DTA mice exhibit a narcoleptic phenotype as previously found (Black et al. 2014; Tabuchi et al. 2014; Black et al. 2016). When a 2 h sleep opportunity occurred after 4 h SD, DTA mice responded with increased percentages of the time spent in NREM, REM, and total sleep time that were comparable to monogenic controls -- indicative of a functional sleep homeostatic response (Table 3 and Fig. 7). Since the proportion of c-FOS[+] nNOS/NK1R neurons directly correlates with NREM sleep time, NREM bout duration and EEG δ power during NREM sleep (Morairty et al. 2013; Dittrich et al. 2015), we determined c-FOS[+]/nNOS expression in both genotypes. We found there were no significant differences in the proportion of c-FOS[+] cortical nNOS cells between DTA and MC mice at either time point studied (Fig. 7). However, these FOS measurements were taken throughout the cortex and were not limited to cingulate cortex nNOS/NK1R neurons. Therefore, although we

saw little effect of Hcrt loss on the electrophysiological properties of nNOS/NK1R cells

of the cingulate cortex in DOX(-) DTA juvenile mice, we cannot rule out that there could

be region-specific differences in c-FOS expression within the cortical nNOS population

affected by the loss of Hcrt innervation.

Perspective

The anatomical, pharmacological and optogenetic data presented here document

that Hcrt neuron projections innervate a subset of cingulate cortex nNOS/NK1R neurons

and that HCRTR1 mediates the excitatory responses in response to HCRT1. The loss

of Hcrt innervation does not appear to greatly influence the activity of cortical

nNOS/NK1R neurons or their expression of c-FOS in response to sleep loss, yet the

electrical response to HCRT1 is lost in tissue taken from sleep-deprived mice.

Therefore, we conclude that Hcrt afferents to cingulate cortex nNOS/NK1R neurons are

unlikely to be involved in sleep homeostasis and the activation of these cells during RS.

Nevertheless, we must express caution in the interpretation of these data due to the

variation in age between mice used for the different experimental paradigms. Adult

mice (2-4 mo) were used for photostimulation of Hcrt terminals and are in the age range

of mice used for the behavioural EEG analysis (2-10 mo), yet the *in vitro* pharmacology

data presented herein was derived from juvenile mice (P14-P28). We have previously

shown that there are no significant changes in electrical properties of cortical

nNOS/NK1 neurons recorded in brain slices between juvenile (P14-P23) and adult (4-6

mo) mice, and that there are comparable GPCR-mediated responses across these ages

(Williams et al. 2017). However, even though the intracellular transduction machinery

underlying a GPCR-mediated response appears to be age-independent, we cannot rule out the possibility that HCRT1 responses on cortical nNOS/NK1R neurons may differ by age.

Considerable evidence suggests that HCRTR2 rather than HCRTR1 is involved in sleep regulation (Willie et al. 2003; Mang et al. 2012; Mieda et al. 2013) whereas HCRTR1 may be involved in addiction and emotionally-motivated behavior (Mahler et al. 2014). The predominant receptor subtype expressed on these nNOS/NK1R neurons, HCRTR1, has been shown to regulate fear conditioning and decision-making in other cortical neurons (Flores et al. 2014). Consequently, we suggest that the Hcrt projection onto cortical nNOS/NK1R cells may facilitate cortical processing of affect in a complementary manner to HCRTR2-expressing layer V pyramidal neurons (Bayer et al. 2004).

References

Ascoli GA, Alonso-Nanclares L, Anderson SA, Barrionuevo G, Benavides-Piccione R, Burkhalter A, Buzsaki G, Cauli B, Defelipe J, Fairen A, Feldmeyer D, Fishell G, Fregnac Y, Freund TF, Gardner D, Gardner EP, Goldberg JH, Helmstaedter M, Hestrin S, Karube F, Kisvarday ZF, Lambolez B, Lewis DA, Marin O, Markram H, Munoz A, Packer A, Petersen CC, Rockland KS, Rossier J, Rudy B, Somogyi P, Staiger JF, Tamas G, Thomson AM, Toledo-Rodriguez M, Wang Y, West DC, Yuste R. 2008. Petilla terminology: nomenclature of features of GABAergic interneurons of the cerebral cortex. Nat Rev Neurosci. 9:557-568.

Bayer L, Serafin M, Eggermann E, Saint-Mleux B, Machard D, Jones BE, Muhlethaler M. 2004. Exclusive postsynaptic action of hypocretin-orexin on sublayer 6b cortical neurons. J Neurosci. 24:6760-6764.

Black SW, Morairty SR, Chen TM, Leung AK, Wisor JP, Yamanaka A, Kilduff TS. 2014. GABAB agonism promotes sleep and reduces cataplexy in murine narcolepsy. J Neurosci. 34:6485-6494.

Black SW, Morairty SR, Fisher SP, Chen TM, Warrier DR, Kilduff TS. 2013. Almorexant promotes sleep and exacerbates cataplexy in a murine model of narcolepsy. Sleep. 36:325-336.

Black SW, Schwartz MD, Chen TM, Hoener MC, Kilduff TS. 2016. Trace Amine-Associated Receptor 1 Agonists as Narcolepsy Therapeutics. Biol Psychiatry.

Cabezas C, Irinopoulou T, Cauli B, Poncer JC. 2013. Molecular and functional characterization of GAD67-expressing, newborn granule cells in mouse dentate gyrus. Front Neural Circuits. 7:60.

Carter ME, Adamantidis A, Ohtsu H, Deisseroth K, de Lecea L. 2009. Sleep homeostasis modulates hypocretin-mediated sleep-to-wake transitions. J Neurosci. 29:10939-10949.

Cauli B, Audinat E, Lambolez B, Angulo MC, Ropert N, Tsuzuki K, Hestrin S, Rossier J. 1997.
Molecular and physiological diversity of cortical nonpyramidal cells. J Neurosci. 17:3894-
3906.

Ch'ng SS, Lawrence AJ. 2015. Distribution of the orexin-1 receptor (OX1R) in the mouse
forebrain and rostral brainstem: A characterisation of OX1R-eGFP mice. J Chem
Neuroanat. 66-67:1-9.

Darwinkel A, Stanic D, Booth LC, May CN, Lawrence AJ, Yao ST. 2014. Distribution of orexin-1
receptor-green fluorescent protein- (OX1-GFP) expressing neurons in the mouse brain
stem and pons: Co-localization with tyrosine hydroxylase and neuronal nitric oxide
synthase. Neuroscience. 278:253-264.

DeFelipe J, Lopez-Cruz PL, Benavides-Piccione R, Bielza C, Larranaga P, Anderson S,
Burkhalter A, Cauli B, Fairen A, Feldmeyer D, Fishell G, Fitzpatrick D, Freund TF,
Gonzalez-Burgos G, Hestrin S, Hill S, Hof PR, Huang J, Jones EG, Kawaguchi Y,
Kisvarday Z, Kubota Y, Lewis DA, Marin O, Markram H, McBain CJ, Meyer HS, Monyer H,
Nelson SB, Rockland K, Rossier J, Rubenstein JL, Rudy B, Scanziani M, Shepherd GM,
Sherwood CC, Staiger JF, Tamas G, Thomson A, Wang Y, Yuste R, Ascoli GA. 2013. New
insights into the classification and nomenclature of cortical GABAergic interneurons. Nat
Rev Neurosci. 14:202-216.

Dittrich L, Heiss JE, Warrier DR, Perez XA, Quik M, Kilduff TS. 2012. Cortical nNOS neurons
co-express the NK1 receptor and are depolarized by Substance P in multiple mammalian
species. Front Neural Circuits. 6:31.

Dittrich L, Morairty SR, Warrier DR, Kilduff TS. 2015. Homeostatic sleep pressure is the primary
factor for activation of cortical nNOS/NK1 neurons. Neuropsychopharmacology. 40:632-
639.

Estabrooke IV, McCarthy MT, Ko E, Chou TC, Chemelli RM, Yanagisawa M, Saper CB,

Scammell TE. 2001. Fos expression in orexin neurons varies with behavioral state. J

Neurosci. 21:1656-1662.

Flores A, Valls-Comamala V, Costa G, Saravia R, Maldonado R, Berrendero F. 2014. The

hypocretin/orexin system mediates the extinction of fear memories.

Neuropsychopharmacology. 39:2732-2741.

Franklin KBJ, Paxinos G. 2008. The Mouse Brain In Stereotaxic Coordinates. Amsterdam:

Elsevier.

Gerashchenko D, Wisor JP, Burns D, Reh RK, Shiromani PJ, Sakurai T, de la Iglesia HO,

Kilduff TS. 2008. Identification of a population of sleep-active cerebral cortex neurons. Proc

Natl Acad Sci U S A. 105:10227-10232.

Gompf HS, Mathai C, Fuller PM, Wood DA, Pedersen NP, Saper CB, Lu J. 2010. Locus

ceruleus and anterior cingulate cortex sustain wakefulness in a novel environment. J

Neurosci. 30:14543-14551.

Hara J, Beuckmann CT, Nambu T, Willie JT, Chemelli RM, Sinton CM, Sugiyama F, Yagami K,

Goto K, Yanagisawa M, Sakurai T. 2001. Genetic ablation of orexin neurons in mice results

in narcolepsy, hypophagia, and obesity. Neuron. 30:345-354.

Hay YA, Andjelic S, Badr S, Lambolez B. 2015. Orexin-dependent activation of layer VIb

enhances cortical network activity and integration of non-specific thalamocortical inputs.

Brain Struct Funct. 220:3497-3512.

Higo S, Akashi K, Sakimura K, Tamamaki N. 2009. Subtypes of GABAergic neurons project

axons in the neocortex. Front Neuroanat. 3:25.

Higo S, Udaka N, Tamamaki N. 2007. Long-range GABAergic projection neurons in the cat

neocortex. J Comp Neurol. 503:421-431.

Jin J, Chen Q, Qiao Q, Yang L, Xiong J, Xia J, Hu Z, Chen F. 2016. Orexin neurons in the
lateral hypothalamus project to the medial prefrontal cortex with a rostro-caudal gradient.
Neurosci Lett. 621:9-14.

Joo EY, Jeon S, Lee M, Kim ST, Yoon U, Koo DL, Lee JM, Hong SB. 2011. Analysis of cortical
thickness in narcolepsy patients with cataplexy. Sleep. 34:1357-1364.

Karagiannis A, Gallopin T, David C, Battaglia D, Geoffroy H, Rossier J, Hillman EM, Staiger JF,
Cauli B. 2009. Classification of NPY-expressing neocortical interneurons. J Neurosci.
29:3642-3659.

Kilduff TS, Cauli B, Gerashchenko D. 2011. Activation of cortical interneurons during sleep: an
anatomical link to homeostatic sleep regulation? Trends Neurosci. 34:10-19.

Kubota Y, Shigematsu N, Karube F, Sekigawa A, Kato S, Yamaguchi N, Hirai Y, Morishima M,
Kawaguchi Y. 2011. Selective coexpression of multiple chemical markers defines discrete
populations of neocortical GABAergic neurons. Cereb Cortex. 21:1803-1817.

Lambe EK, Aghajanian GK. 2003. Hypocretin (orexin) induces calcium transients in single
spines postsynaptic to identified thalamocortical boutons in prefrontal slice. Neuron.
40:139-150.

Lambolez B, Audinat E, Bochet P, Crepel F, Rossier J. 1992. AMPA receptor subunits
expressed by single Purkinje cells. Neuron. 9:247-258.

Madisen L, Zwingman TA, Sunkin SM, Oh SW, Zariwala HA, Gu H, Ng LL, Palmiter RD,
Hawrylycz MJ, Jones AR, Lein ES, Zeng H. 2010. A robust and high-throughput Cre
reporting and characterization system for the whole mouse brain. Nat Neurosci. 13:133-
140.

Mahler SV, Moorman DE, Smith RJ, James MH, Aston-Jones G. 2014. Motivational activation: a
unifying hypothesis of orexin/hypocretin function. Nat Neurosci. 17:1298-1303.

Mang GM, Durst T, Burki H, Imobersteg S, Abramowski D, Schuepbach E, Hoyer D, Fendt M, Gee CE. 2012. The dual orexin receptor antagonist almorexant induces sleep and decreases orexin-induced locomotion by blocking orexin 2 receptors. Sleep. 35:1625-1635.

Mendlewicz J. 2009. Sleep disturbances: core symptoms of major depressive disorder rather than associated or comorbid disorders. World J Biol Psychiatry. 10:269-275.

Mieda M, Tsujino N, Sakurai T. 2013. Differential roles of orexin receptors in the regulation of sleep/wakefulness. Front Endocrinol (Lausanne). 4:57.

Mishima K, Fujiki N, Yoshida Y, Sakurai T, Honda M, Mignot E, Nishino S. 2008. Hypocretin receptor expression in canine and murine narcolepsy models and in hypocretin-ligand deficient human narcolepsy. Sleep. 31:1119-1126.

Mochizuki T, Crocker A, McCormack S, Yanagisawa M, Sakurai T, Scammell TE. 2004. Behavioral state instability in orexin knock-out mice. J Neurosci. 24:6291-6300.

Morairty SR, Dittrich L, Pasumarthi RK, Valladao D, Heiss JE, Gerashchenko D, Kilduff TS. 2013. A role for cortical nNOS/NK1 neurons in coupling homeostatic sleep drive to EEG slow wave activity. Proc Natl Acad Sci U S A. 110:20272-20277.

Pasumarthi RK, Gerashchenko D, Kilduff TS. 2010. Further characterization of sleep-active neuronal nitric oxide synthase neurons in the mouse brain. Neuroscience. 169:149-157.

Paul A, Crow M, Raudales R, He M, Gillis J, Huang ZJ. 2017. Transcriptional Architecture of Synaptic Communication Delineates GABAergic Neuron Identity. Cell. 171:522-539 e520.

Peyron C, Faraco J, Rogers W, Ripley B, Overeem S, Charnay Y, Nevsimalova S, Aldrich M, Reynolds D, Albin R, Li R, Hungs M, Pedrazzoli M, Padigaru M, Kucherlapati M, Fan J, Maki R, Lammers GJ, Bouras C, Kucherlapati R, Nishino S, Mignot E. 2000. A mutation in a case of early onset narcolepsy and a generalized absence of hypocretin peptides in human narcoleptic brains. Nat Med. 6:991-997.

Peyron C, Tighe DK, van den Pol AN, de Lecea L, Heller HC, Sutcliffe JG, Kilduff TS. 1998. Neurons containing hypocretin (orexin) project to multiple neuronal systems. J Neurosci. 18:9996-10015.

Rolls ET, Inoue K, Browning A. 2003. Activity of primate subgenual cingulate cortex neurons is related to sleep. J Neurophysiol. 90:134-142.

Sasaki K, Suzuki M, Mieda M, Tsujino N, Roth B, Sakurai T. 2011. Pharmacogenetic modulation of orexin neurons alters sleep/wakefulness states in mice. PLoS One. 6:e20360.

Scammell TE, Willie JT, Guilleminault C, Siegel JM, International Working Group on Rodent Models of N. 2009. A consensus definition of cataplexy in mouse models of narcolepsy. Sleep. 32:111-116.

Tabuchi S, Tsunematsu T, Black SW, Tominaga M, Maruyama M, Takagi K, Minokoshi Y, Sakurai T, Kilduff TS, Yamanaka A. 2014. Conditional ablation of orexin/hypocretin neurons: a new mouse model for the study of narcolepsy and orexin system function. J Neurosci. 34:6495-6509.

Tabuchi S, Tsunematsu T, Kilduff TS, Sugio S, Xu M, Tanaka KF, Takahashi S, Tominaga M, Yamanaka A. 2013. Influence of inhibitory serotonergic inputs to orexin/hypocretin neurons on the diurnal rhythm of sleep and wakefulness. Sleep. 36:1391-1404.

Tafti M, Villemin E, Carlander B, Besset A, Billiard M. 1992. Sleep in human narcolepsy revisited with special reference to prior wakefulness duration. Sleep. 15:344-351.

Taniguchi H, He M, Wu P, Kim S, Paik R, Sugino K, Kvitsiani D, Fu Y, Lu J, Lin Y, Miyoshi G, Shima Y, Fishell G, Nelson SB, Huang ZJ. 2011. A resource of Cre driver lines for genetic targeting of GABAergic neurons in cerebral cortex. Neuron. 71:995-1013.

Tasic B, Menon V, Nguyen TN, Kim TK, Jarsky T, Yao Z, Levi B, Gray LT, Sorensen SA, Dolbeare T, Bertagnolli D, Goldy J, Shapovalova N, Parry S, Lee C, Smith K, Bernard A, Madisen L, Sunkin SM, Hawrylycz M, Koch C, Zeng H. 2016. Adult mouse cortical cell taxonomy revealed by single cell transcriptomics. Nat Neurosci. 19:335-346.

Thannickal T, Moore R, Y., Nienhuis R, Ramanathan L, Gulyani S, Aldrich M, Cornford M, Siegel JM. 2000. Reduced number of hypocretin neurons in human narcolepsy. Neuron. 27:469-474.

Tomioka R, Okamoto K, Furuta T, Fujiyama F, Iwasato T, Yanagawa Y, Obata K, Kaneko T, Tamamaki N. 2005. Demonstration of long-range GABAergic connections distributed throughout the mouse neocortex. Eur J Neurosci. 21:1587-1600.

Tomioka R, Rockland KS. 2007. Long-distance corticocortical GABAergic neurons in the adult monkey white and gray matter. J Comp Neurol. 505:526-538.

Tripp A, Kota RS, Lewis DA, Sibille E. 2011. Reduced somatostatin in subgenual anterior cingulate cortex in major depression. Neurobiol Dis. 42:116-124.

Wenger Combremont AL, Bayer L, Dupre A, Muhlethaler M, Serafin M. 2016a. Effects of Hypocretin/Orexin and Major Transmitters of Arousal on Fast Spiking Neurons in Mouse Cortical Layer 6B. Cereb Cortex. 26:3553-3562.

Wenger Combremont AL, Bayer L, Dupre A, Muhlethaler M, Serafin M. 2016b. Slow Bursting Neurons of Mouse Cortical Layer 6b Are Depolarized by Hypocretin/Orexin and Major Transmitters of Arousal. Front Neurol. 7:88.

Williams RH, Alexopoulos H, Jensen LT, Fugger L, Burdakov D. 2008. Adaptive sugar sensors in hypothalamic feeding circuits. Proc Natl Acad Sci U S A. 105:11975-11980.

Williams RH, Chee MJ, Kroeger D, Ferrari LL, Maratos-Flier E, Scammell TE, Arrigoni E. 2014. Optogenetic-mediated release of histamine reveals distal and autoregulatory mechanisms for controlling arousal. J Neurosci. 34:6023-6029.

Williams RH, Vazquez-DeRose J, Thomas AM, Piquet J, Cauli B, Kilduff TS. 2017. Cortical nNOS/NK1 Receptor Neurons are Regulated by Cholinergic Projections From the Basal Forebrain. Cereb Cortex.1-21.

Willie JT, Chemelli RM, Sinton CM, Tokita S, Williams SC, Kisanuki YY, Marcus JN, Lee C, Elmquist JK, Kohlmeier KA, Leonard CS, Richardson JA, Hammer RE, Yanagisawa M.

2003. Distinct narcolepsy syndromes in Orexin receptor-2 and Orexin null mice: molecular genetic dissection of Non-REM and REM sleep regulatory processes. Neuron. 38:715-730.

Yan XX, Garey LJ. 1997. Morphological diversity of nitric oxide synthesising neurons in mammalian cerebral cortex. J Hirnforsch. 38:165-172.

Zeisel A, Munoz-Manchado AB, Codeluppi S, Lonnerberg P, La Manno G, Jureus A, Marques S, Munguba H, He L, Betsholtz C, Rolny C, Castelo-Branco G, Hjerling-Leffler J, Linnarsson S. 2015. Brain structure. Cell types in the mouse cortex and hippocampus revealed by single-cell RNA-seq. Science. 347:1138-1142.

Table 1. Names and characteristics of transgenic mouse lines used in the present study.

Name	Definition / Official Name / Source / RRID	Characteristics and Use in the Present Study
C57Bl/6J	Jackson Laboratories strain #000664; RRID:IMSR_JAX:000664	Wild type (WT) mice used for breeding, *in vitro* electrophysiological slice recordings, to assess viral expression and penetrance, and for single cell RT-PCR.
nNOS-CreER	B6;129S-*Nos1*$^{tm1.1(cre/ERT2)Zjh}$/J; Jackson Laboratories strain #014541; RRID:IMSR_JAX:014541	Originally described by Taniguchi et al. (2011). When injected with tamoxifen, a ligand for the estrogen receptor (ER), Cre recombinase is induced specifically in neurons that express neuronal nitric oxide synthase (nNOS). In the present study, *nNOS-CreER* mice were used for breeding.
Ai14	B6;129S6-*Gt(ROSA)26Sor*$^{tm14(CAG-tdTomato)Hze}$/J Jackson Laboratories strain #007914; RRID:IMSR_JAX:007914	Originally described by Madisen et al. (2010), this reporter strain expresses the red fluorescent protein tdTomato. In the present study, *Ai14* mice were used for breeding with *nNOS-CreER mice.*
nNOS-CreER;Ai14		Bigenic mice generated by breeding *nNOS-CreER* mice with *Ai14* mice. In the resultant progeny, nNOS neurons express tdTomato. In the present study, *nNOS-CreER;Ai14* mice were used for breeding with *Orexin-tTA mice.*
Orexin-tTA	Orexin-tetracycline-controlled Transcriptional Activator ("*ox-tTA*" mice)	"*Ox-tTA*" mice were originally described by Tabuchi et al. (2013). In this strain, tTA, driven by human prepro-orexin promoter, is exclusively expressed in Hcrt/orexin neurons. In the present study, *Ox-tTA* mice were used for breeding, to assess viral expression and penetrance, to express ChR2 in Hcrt cells for *in vitro* electrophysiological slice recordings of both Hcrt and nNOS cells, and as monogenic littermate controls in the EEG studies.
Orexin-tTA; nNOS-CreER;Ai14	"*Ox-tTA;nNOS-CreER;Ai14*" mice	Trigenic "*ox-tTA;nNOS-CreER;Ai14*" mice were generated by breeding *Orexin-tTA mice with* bigenic *nNOS-CreER;Ai14* mice. In the present study, *ox-tTA;nNOS-CreER;Ai14* mice were injected with an AAV encoding TetO-ChR2 and then used for *in vitro* optogenetic stimulation of Hcrt terminals and recording of cortical nNOS cells.
Orexin-tTA; TetO-DTA	Orexin-tetracycline-controlled Transcriptional Activator; Tetracycline Operator 5; Diphtheria Toxin A fragment ("*DTA*" mice)	These bigenic "*DTA*" mice were described by Tabuchi et al. (2014). tTA is exclusively expressed in Hcrt/orexin neurons. In the absence of doxycycline in the chow ("DOX(-)"), tTA binds to *TetO* and induces production of the toxic DTA protein in the Hcrt neurons which results in degeneration of these cells. In the present study, *DTA* mice were used for *in vitro* electrophysiology, immunohistochemistry and EEG/EMG recording.
Hcrtr1-EGFP	Hypocretin Receptor 1-Enhanced Green Fluorescent Protein. Mutant Mouse Regional Resource Center RRID:MMRRC_030803-UCD	Originally described in Darwinkel et al. (2014), the founder line (KP68Gsat/Mmucd) was from the Mutant Mouse Regional Resource Center. EGFP was inserted upstream of the Hcrtr1 gene. In the present study, *Hcrtr1-EGFP* mice were used for immunohistochemistry.

Table 2. PCR primers used to amplify GABA interneuron markers and hypocretin receptor mRNAs

Gene Accession #	First PCR primers	Size (bp)	Second PCR nested primers	Size (bp)
GAD65 NM_008078	Sense, 99: CCAAAAGTTCACGGGCGG (Cabezas et al. 2013) Antisense, 454: TCCTCCAGATTTTGCGGTTG (Cabezas et al. 2013)	375	Sense, 219: CACCTGCGACCAAAAACCCT (Cabezas et al. 2013) Antisense, 447: GATTTTGCGGTTGGTCTGCC (Cabezas et al. 2013)	248
GAD67 NM_008077	Sense, 529: TACGGGGTTCGCACAGGTC (Cabezas et al. 2013) Antisense, 1109: CCCAGGCAGCATCCACAT (Cabezas et al. 2013)	598	Sense, 801: CCCAGAAGTGAAGACAAAAGGC (Cabezas et al. 2013) Antisense, 1034: AATGCTCCGTAAACAGTCGTGC (Cabezas et al. 2013)	255
SOM NM_009215	Sense, 43: ATCGTCCTGGCTTTGGGC (Cauli et al. 1997) Antisense, 231: GCCTCATCTCGTCCTGCTCA (Cauli et al. 1997)	208	Sense, 75: GCCCTCGGACCCCAGACT (Gallopin et al. 2006) Antisense, 203: GCAAATCCTCGGGCTCCA	146
NPY NM_023456	Sense, 16: CGAATGGGGCTGTGTGGA (Cabezas et al. 2013) Antisense, 286: AAGTTTCATTTCCCATCACCACAT (Cabezas et al. 2013)	294	Sense, 38: CCCTCGCTCTATCTCTGCTCGT (Cabezas et al. 2013) Antisense, 236: GCGTTTTCTGTGCTTTCCTTCA (Cabezas et al. 2013)	220
nNOS NM_008712	Sense, 3009: GCAAAGTCCTAAATCCAGCCGA Antisense, 3403: TGCCCCATTTCCATTCCTCATA	416	Sense, 3034: ACCATCTTCGTGCGTCTCCA Antisense, 3346: GCTTCTCTTTCTCATTGGTGGC (Williams et al. 2017)	334
NK1R NM_009313	Sense, 30: TCTCTTCCCCAACACCTCCA Antisense, 459: GGAGAGCCAGGACCCAGATG (Williams et al. 2017)	449	Sense, 123: CATCGTGGTGACTTCCGTGG Antisense, 397: TGAAGAGGGTGGATGATGGC (Williams et al. 2017)	294
SOM intron X51468	Sense, 8: CTGTCCCCCTTACGAATCCC (Cabezas et al. 2013) Antisense, 228: CCAGCACCAGGGATAGAGCC (Cabezas et al. 2013)	240	Sense, 16: CTTACGAATCCCCCAGCCTT (Cabezas et al. 2013) Antisense, 178:TTGAAAGCCAGGGAGGAACT (Cabezas et al. 2013)	182
vGLUT1 NM_182993	Sense, -113: GGCTCCTTTTTCTGGGGCTAC Antisense, 126: CCAGCCGACTCCGTTCTAAG (Cabezas et al. 2013)	259	Sense, -54: ATTCGCAGCCAACAGGGTCT Antisense, 79: TGGCAAGCAGGGTATGTGAC (Cabezas et al. 2013)	153
HcrtR1 NM_198959.2	Sense, 876: TCGGAGGAAGACGGCTAAGA Antisense, 1185: TTGGAGACGGAGCAGCGG	327	Sense, 895: ATGCTGATGGTAGTCCTGCTGG Antisense, 1111: GCAGCAGGAGAAGGCAGC	234
HcrtR2 NM_198962	Sense, 786: TCAGAGAAAATGGAAGCAGCAG Antisense, 1129: CAAGACAACAAGAAAAGGCAGC	365	Sense, 861: CGCTGTTGCTGCTGAGATAAAG Antisense, 1033: GCCAATGAGAAAAAGTGAACCA	194

Note: Position 1, first base of the start codon.

Table 3. Sleep parameters and c-FOS expression in cortical nNOS/NK1R neurons

| | Sleep Deprivation | | Recovery Sleep | | | |
	MC ($n = 4$)	DTA ($n = 5$)	MC ($n = 3$)	DTA ($n = 7$)	Two-way ANOVA	P
Total Sleep % Time	2.2 ± 1.0	3.5 ± 1.5	83.3 ± 1.7	71.7 ± 4.9	$F_{(1, 15)} = 336.2$	0.0001
NREM % Time	2.2 ± 1.0	3.5 ± 1.5	77.8 ± 3.6	68.7 ± 4.7	$F_{(1, 15)} = 313.48$	0.0001
REM % Time	0	0	5.6 ± 1.9	3.0 ± 0.7	$F_{(1,15)} = 27.79$	0.0001
Cataplexy % Time	0	1.9 ± 1.1	0	0.5 ± 0.2	$F_{(1, 15)} = 1.25$	*n.s.*
NREM δ Power (μV^2)	0	182.1 ± 96.9	397.4 ± 128.7	377.8 ± 79.2	$F_{(1,15)} = 10.35$	0.0058
% c-FOS/nNOS	11.5 ± 1.5	14.0 ± 1.4	76.7 ± 2.3	72.7 ± 4.1	$F_{(1,14)} = 274.71$	0.0001

data are mean ± S.E.M.

MC, monogenic controls; DTA, *orexin/tTA;TetO-DTA* mice

bold font = main effect for sleep condition; no interaction or effect of genotype

Figure Legends

Figure 1. Electrophysiological responses of cortical nNOS/NK1R cells to bath application of HCRT1/orexin-A. A. (**i**) Schematic illustrating experimental approach underlying *in vitro* electrophysiological studies of cortical nNOS/ NK1R cells (**ii**) in the deep layers of the cingulate cortex. (**iii**) Cortical nNOS/NK1R neurons were identified by application of SP-TMR, a fluorescent agonist for the NK1R (scale bar = 25 µm). **B**. Bath application of hypocretin 1 (HCRT1; 100 nM) evoked an inward current and membrane depolarization (**C**). In the presence of tetrodotoxin (TTX; 1 µM), both the voltage-clamp (**D**) and current-clamp (**E**) responses persisted. To confirm a postsynaptic mechanism of action, HCRT1 was applied in the presence of glutamatergic (CNQX,7 µM; AP5, 100 µM) and GABAergic (2-HS, 5 µM; BIC, 10 µM) blockers, TTX and 0 Ca^{2+}/ 3.3 Mg^{2+}-containing aCSF (**F-G**). Summary of the HCRT1-evoked current (**H**) and membrane depolarization (**I**) on cortical nNOS/NK1R neurons. There were no statistically significant differences between HCRT1 application in normal aCSF, in the presence of TTX, or in 0 Ca^{2+}/ 3.3 Mg^{2+}-containing aCSF conditions in either voltage-clamp (one-way ANOVA, $F_{(2,32)}$ = 0.90, P = 0.41) or current-clamp conditions (one-way ANOVA, $F_{(2,21)}$ = 0.76, P = 0.48). However, after 4 h sleep deprivation, *ex vivo* cortical nNOS cells had no significant responses to HCRT1 application. The absence of a response was significantly different from that evoked in non-sleep deprived mice in TTX-aCSF for current (unpaired *t*-test, $t_{(18)}$ = 2.90, P = 0.009) and membrane depolarization (unpaired *t*-test, $t_{(10)}$ = 2.49, P = 0.03).

Figure 2. HCRT1 effects are primarily mediated by the expression of HCRTR1 on cortical nNOS/NK1R neurons. A. Pre-application of the HCRTR1 receptor antagonist SB-334867 (SB; 10 nM) significantly reduced the HCRT1-evoked inward current by ~63% (n = 5) whereas the HCRTR2 receptor antagonist TCS OX2 29 (TCS; 10nM) had no significant effect (~4% reduction, n = 4; one-way ANOVA with Newman-Keuls *post hoc* test). Co-application of both antagonists also blocked the current response (one-way ANOVA, $P < 0.0001$; n = 8). **B**. In current-clamp, pre-application of TCS OX2 29 had little effect on HCRT1-mediated depolarization but SB-334867 and co-application of both antagonists significantly reduced the change in membrane potential by ~77% and 81%, respectively (one-way ANOVA with Newman-Keuls *post hoc* test, $P < 0.0001$). **C.** Tissue sections from a *Hcrtr1-EGFP* mouse brain indicated HCRTR1 expression in the cingulate cortex (top row; scale bar = 5 μm) and in nNOS neurons (white arrows). Enlarged inset (bottom row) illustrates HCRTR1 expression in a cortical nNOS neuron. **D.** Single cell RT-PCR of cortical nNOS/NK1R neurons, confirmed by colocalization of biocytin with nNOS immunostaining (inset), demonstrated that ~31% of cortical nNOS/NK1R neurons express *Hcrtr1* mRNA but none were positive for *Hcrtr2* mRNA (**G**; n = 13; scale bar = 12 μm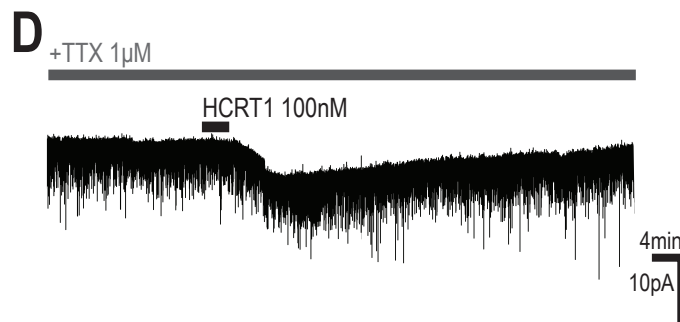). [***, $P < 0.001$; **, $P < 0.01$; *, $P < 0.05$; *n.s.*, non-significant; one-way ANOVA; DAPI, 4',6-diamidino-2-phenylindole; GFP, green fluorescent protein; *Slc17a7* for VGlut1; *Gad2* for GAD65; *Gad1* for GAD67; *Sst* for SOM; *Nos1* for nNOS; *Tacr1* for NK1R]

Figure 3. HCRT1 effects on glutamatergic inputs onto cortical nNOS/NK1R neurons. Bath application of HCRT1 significantly reduced spontaneous excitatory

postsynaptic currents (sEPSCs) onto cortical nNOS/NK1R neurons (**A**; 80.85 ± 1.93%, RM-ANOVA, $F_{(2,20)}$ = 12.49, P = 0.001). In contrast, HCRT1 did not significantly affect miniature EPSC (mEPSC) activity (**B**; RM-ANOVA, $F_{(2,20)}$ = 0.59, P = 0.57). Pre-application of SB-334867 (+SB) resulted in HCRT1 evoking an increase in mEPSC activity (RM-ANOVA, $F_{(2,20)}$ = 13.34, P = 0.0027; **C**), as did TCS-OX2-29 (+TCS; RM-ANOVA, $F_{(2,20)}$ = 7.93, P = 0.0006; **D**). When both antagonists were pre-applied (++SB/TCS), HCRT1 bath application did not significantly change mEPSC frequency (RM-ANOVA, $F_{(2,20)}$ = 1.43, P = 0.28; **E**). [***, P < 0.001; **, P < 0.01; *, P < 0.05; *n.s.*, non-significant; one-way ANOVA]

Figure 4. Expression of channelrhodopsin-2 (ChR2) in Hcrt-containing LHA neurons and cortical projections. A. Schematics illustrating the bilateral injection of a TetO-dependent channelrhodopsin (AAV(DJ)-TetO-ChR2(ET/TC)-eYFP) virus into the lateral hypothalamic area (LHA) of *ox-tTA* mice (left) to target expression to Hcrt neurons which were subsequently recorded to determine ChR2 activation kinetics (right). **Bi**. Temporal dynamics and sensitivity of the ChR2 opsin to blue light (470 nm) stimulation (2ms pulse width) was evaluated in voltage-clamp and current-clamp mode. (**ii**) A patched ChR2-expressing cell and the resultant current and electrical firing with 10ms pulse-width blue-light application. **C.** Immunohistochemical confirmation of ChR2 (GFP; green) expression within Hcrt-expressing (HCRT1 & 2; magenta) neurons of the LHA at different magnifications (scale bar = 250 μm, unless otherwise stated). Examples of colocalized cells at higher magnification (white arrows). **D.** In *ox-tTA;nNOS-CreER;Ai14* mice, ChR2 was expressed within Hcrt neurons of the LHA (**i;**

white arrows), and ChR2 was expressed in LHA projections to the cingulate cortex within proximity of nNOS/NK1R neurons (**ii**). [3V, third ventricle; f, fornix]

Figure 5. Optogenetic stimulation of hypocretinergic afferents to cingulate cortex nNOS/NK1R neurons. Ai. Schematic illustrating stimulation of Hcrt afferent terminals onto cingulate cortex nNOS/NK1R neurons. Blue light stimulation of Hcrt terminal afferents onto cortical nNOS/NK1R neurons resulted in small inward currents (**iii**, two cells illustrated) and an increase in glutamatergic input following light stimulation (**iv**). Photo-evoked currents in normal aCSF (top) and TTX (1 µM) plus 4-aminopyridine (4-AP, 0.5 µM; bottom) conditions were significant in a small proportion of recorded nNOS/NK1R neurons ('black' circles; **v**). **B**. Temporal analysis indicated that some cells (*n* = 4 of 13) exhibited a time-locked EPSC response to blue light stimulation (10 ms pulse width; 1Hz, repeated 30 times). Top panel shows the averaged response in 'blue' for one cell during the photostimulation protocol, while overall sEPSC$_o$ activity increased significantly (RM-ANOVA with Newman-Keuls *post hoc* test, $F_{(2,10)}$ = 10.16, *P* = 0.004; K-S test < 0.00001). Bottom panel in B, C and D presents a schematic to summarize the results. **C**. In the presence of TTX + 4-AP, few time-locked EPSCs were observed but a significant increase in mEPSC$_o$ frequency occurred (RM-ANOVA with Newman-Keuls *post hoc* test, $F_{(2,10)}$ = 2.65, *P* = 0.0009). **D**. When blue-light stimulation was repeated in the presence of the HCRTR1 and HCRTR2 antagonists, SB-334867 (SB; 10 µM) and TCS OX2 29 (TCS; 10 µM) respectively, the increase in mEPSC$_o$ frequency was blocked (RM-ANOVA with Newman-Keuls *post hoc* test, $F_{(2,10)}$

= 0.37, P = 0.7). [***, $P < 0.001$; **, $P < 0.01$; *, $P < 0.05$; *n.s.*, non-significant; one-way ANOVA; latV, lateral ventricle]

Figure 6. **Response of cortical nNOS/NK1R neurons to HCRT1 application is affected in mice depleted of Hcrt neurons. Ai**. Doxycycline (DOX) was removed from the diet (DOX(-)) of *Orexin-tTA;DTA* (*ox-tTA;DTA*) adult mice to induce Hcrt neuron degeneration and then paired for breeding. The resultant *Ox-tTA;DTA* offspring were used at P14-21 for histology and for whole-cell patch clamp electrophysiological recordings of cortical nNOS/NK1R neurons. (**ii**) Histological comparison of aged-matched DOX(+) and DOX(-) pups indicated significant degeneration of Hcrt neurons in the DOX(-) condition. **B.** When basal sEPSC activity was compared between WT and DOX(-) *ox-tTA;DTA* pups (DTA), there was a significant increase in the amplitude of events in DTA mice compared to WT (unpaired *t*-test, $t_{(398)}$ = 6.55, $P < 0.0001$; n = 9 vs 11, respectively) but no difference in the frequency of the events (unpaired *t*-test, $t_{(18)}$ = 0.97, P = 0.34). **C.** In contrast, there was a significant decrease in basal mEPSC frequency when DOX(-) DTA mice were compared to WT mice (unpaired *t*-test, $t_{(17)}$ = 2.12, P = 0.04; n = 7 vs 13, respectively) as well as an increase in mEPSC amplitude (unpaired *t*-test, $t_{(398)}$ = 3.25, P = 0.001). **D.** When HCRT1 (100 nM) was bath applied to cortical nNOS/NK1R neurons of DOX(-) DTA mice, there was very little current evoked in voltage-clamp in the majority of cells (n = 2 of 7; **i**) and little membrane depolarization in current-clamp recordings (not shown). Examples of sEPSC activity of cortical nNOS/NK1R neurons from DOX(-) DTA mice (**ii**). **Diii.** Bath application of HCRT1 significantly reduced sEPSC activity (~20%) onto cortical nNOS/NK1R neurons

(RM-ANOVA, $F_{(2,12)}$ = 5.40, P = 0.020). **E**. In TTX, HCRT1 evoked a significant inward current in one neuron (**i**) but did not affect the activity of mEPSC activity (**ii-iii**) onto cortical nNOS/NK1R cells (one-way ANOVA, P = 0.38; n = 4).

Figure 7. Loss of Hcrt innervation does not affect sleep parameters related to sleep homeostasis or c-FOS expression in cortical nNOS/NK1R neurons. A. Immunohistochemical analysis of c-FOS and cortical nNOS/NK1R neurons from adult *Ox-tTA;DTA* (DTA) mice and monogenic controls (MC) implanted for EEG (scale bar = 50 µm). **B.** Neither NREM delta energy (NRDE; left panel) recorded during a 2 h recovery sleep (RS) period after a 4 h sleep deprivation (SD), nor the proportion of c-FOS+ cortical nNOS neurons (right panel) differed between the two mouse strains. For NRDE, two-way ANOVA revealed a significant main effect of "sleep condition" ($F_{(1,14)}$ = 21.30, P = 0.0003) without a significant effect of genotype or a genotype x condition interaction. Sleep condition was also significant for c-FOS colocalization in cortical nNOS neurons ($F_{(1,14)}$ = 274.71, P = 0.0001) without an effect of genotype or an interaction. [Sleep deprivation, SD; Recovery sleep, RS]

A

i cortical layer V-VI

nNOS

HCRT

ii

iii SP-TMR   DIC

B HCRT1 100nM

3min
10pA

C HCRT1 100nM

-71mV

5min
5mV

D +TTX 1μM

HCRT1 100nM

4min
10pA

E +TTX 1μM

HCRT1 100nM

-64mV

5min
5mV

F 0mM Ca / 3.3mM Mg; Glu and GABA antags; TTX

HCRT1 100nM

4min
10pA

G 0mM Ca / 3.3mM Mg; Glu and GABA antags; TTX

HCRT1 100nM

-64mV

5min
4mV

H

ΔI_{HCRT-1} (pA)

(10)   (17)   (6)   (3)

**   ***   *   n.s.

HCRT1   +TTX   +TTX   +4hr SD
                  0Ca/3.3Mg
                  Glu & GABA$_{antags}$

I

ΔVm_{HCRT-1} (mV)

**   ***   **   n.s.

(9)   (9)   (4)   (3)

HCRT1   +TTX   +TTX   +4hr SD
                  0Ca/3.3Mg
                  Glu & GABA$_{antags}$

A

SB 334867 (10nM) — HCRTR1 / HCRTR2 — TCS OX2 29 (10nM)

G_q $G_{q \text{ or } i/o}$

ΔI_{HCRT-1} (pA)

(9) (5)* (4) (9)***

+TTX +SB +TCS +TCS +SB

B

ΔVm_{HCRT-1} (mV)

(9) (4)** (4) (8)*

+TTX +SB +TCS +TCS +SB

C

nNOS GFP | nNOS | GFP

nNOS GFP | nNOS | GFP

25μm

D

Biocytin DAPI nNOS

31% HCRTR1   0% HCRTR2

Φ Slc17a7 Gad2 Gad1 Sst Npy Nos1 Tacr1 Hcrtr1 Hcrtr2

A

HCRT1 100nm

Baseline

+HCRT1 100nm

Wash

ΔsEPSC$_{HCRT-1}$ freq (%)

BL HCRT W

(6) (6) (6)

**

ΔsEPSC$_{HCRT-1}$ freq (%)

Time (min)
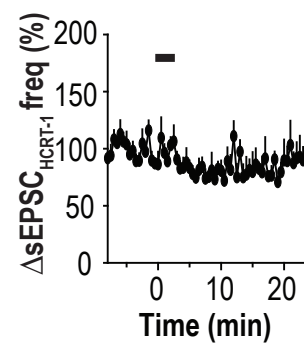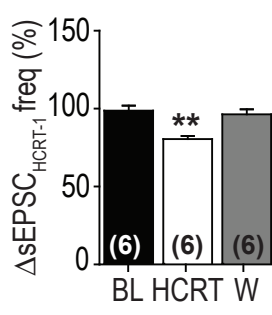
B

+TTX 1µM

Baseline

+HCRT1 100nm

Wash

ΔmEPSC$_{HCRT-1}$ freq (%)

n.s.

BL HCRT W

(14) (14) (14)

ΔmEPSC$_{HCRT-1}$ freq (%)

Time (min)
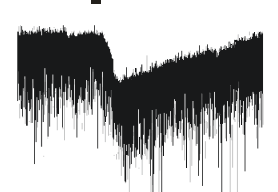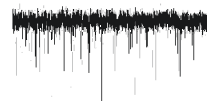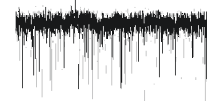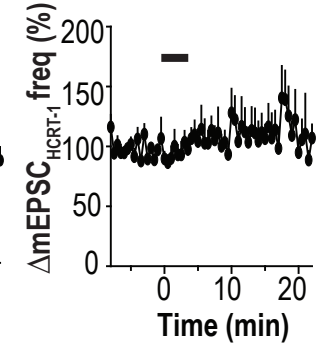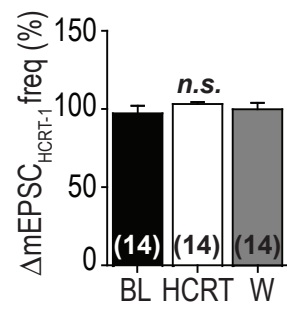
C

++SB 334867 10µM

+SB

+HCRT1 100nm

Wash

ΔmEPSC$_{HCRT-1}$ freq (%)

**

BL HCRT W
     +SB

(5) (5) (5)

ΔmEPSC$_{HCRT-1}$ freq (%)

++SB 334867 10µM

Time (min)
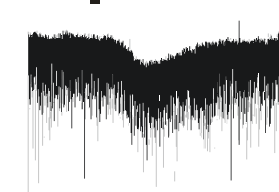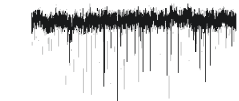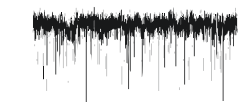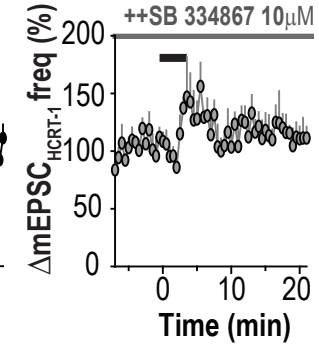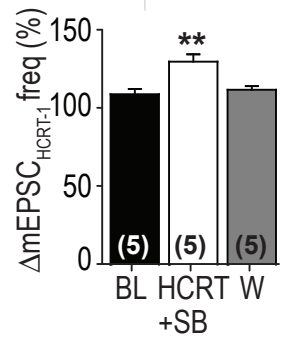
D

++TCS OX2 29 10µM

+TCS

+HCRT1 100nm

Wash

ΔmEPSC$_{HCRT-1}$ freq (%)

**

BL HCRT W
     +TCS

(3) (3) (3)

ΔmEPSC$_{HCRT-1}$ freq (%)

++TCS OX2 29 10µM

Time (min)
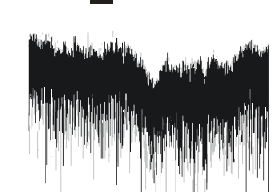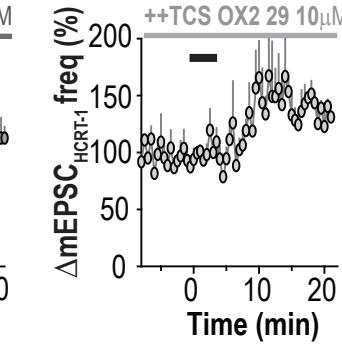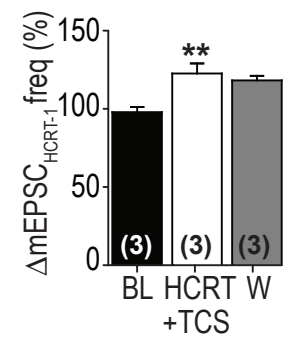
E

++SB 334867 10µM
++TCS OX2 29 10µM

+SB/TCS

+HCRT1 100nm

Wash

ΔmEPSC$_{HCRT-1}$ freq (%)

n.s.

BL HCRT W
     +SB/TCS

(7) (7) (7)

ΔmEPSC$_{HCRT-1}$ freq (%)

++SB/TCS

Time (min)

A

TetO-ChR2

lateral hypothalamic area

ox-tTA

470nm

HCRT

B

i 2ms pulse width

ΔI evoked (pA) / ΔVm (mV)

LED power stimulus: 1% 2% 5% 10% 50% 100%

(4) (6) (6) (7) (7) (7)
(6) (7) (6) (5) (6) (6)

ii 10ms pulse width; 1Hz

200pA

20mV

3V

f

C

HCRT1 & 2 / GFP   HCRT1 & 2   GFP

f

HCRT1 & 2 / GFP   HCRT1 & 2   GFP

f

30um

HCRT1 & 2 / GFP   HCRT1 & 2   GFP

D

i

30um

HCRT1 & 2 / GFP / tdtomato   tdtomato   HCRT1 & 2   GFP

ii

12um

HCRT1 & 2 / GFP / tdtomato   tdtomato   HCRT1 & 2   GFP

A

i cortical layer V-VI
470nm

nNOS
glutamate
GABA
HCRT
HCRT

ox-tTA;nNOS-CreER;Ai14

ii
latV

iii normal aCSF
a   b   c   d
2min
20pA

TTX + 4-AP
e f   g   h
5min
20pA

10ms pulse width; 1Hz

iv
a
b
c
d
20pA

e
f
g
h
20pA

v normal aCSF
I_o (pA)
pre   stim

TTX + 4-AP
I_o (pA)
pre   stim

B sEPSC
10pA

31
21
Trials
11
1
0 10 20 30 40 50 60 70 80 90 100
Time (ms)

sEPSC$_o$ freq (%)
250
200
150
100
50
0 10 20
Time (min)

150   **
100
50
(13) (13) (13)
BL Stim W

Hcrt
?
Glu
nNOS/NK1R
HCRTR1
HCRTR2

C mEPSC
TTX + 4-AP

31
21
Trials
11
1
0 10 20 30 40 50 60 70 80 90 100
Time (ms)

mEPSC$_o$ freq (%)
250   +4-AP
200
150
100
50
0 10 20
Time (min)

150   *
100
50
(7) (7) (7)
BL Stim W

Hcrt
?
TTX X
nNOS/NK1R
HCRTR1
HCRTR2
Hcrt
Glu Glu

D mEPSC
TTX + 4-AP with antagonists

31
21
Trials
11
1
0 10 20 30 40 50 60 70 80 90 100
Time (ms)

mEPSC$_o$ freq (%)
250   +SB/TCS
200
150
100
50
0 10 20
Time (min)

150   *n.s.*
100
50
(7) (7) (7)
BL Stim W

Hcrt
?
TTX X
nNOS/NK1R
SB 334867
HCRTR1
HCRTR2
TCS OX2 29
Hcrt

A

i *ox-tTA; TetO-DTA*
DOX (-)

cortical layer V-VI nNOS

HCRT

ii

DOX (+)

DOX (-)

50μm

B

sEPSC frequency (Hz)

WT (11) DTA (9)

sEPSC amplitude (pA)

WT DTA ***

C

mEPSC frequency (Hz)

WT (12) DTA (7) *

mEPSC amplitude (pA)

WT DTA **

D

i HCRT1 100nM

2min
10pA

ii Baseline

+HCRT1 100nm

Wash

5pA
5s

iii

ΔsEPSC$_{HCRT-1}$ freq (%)

Time (min)

ΔsEPSC$_{HCRT-1}$ freq (%)

BL HCRT ** W
(4) (4) (4)

E

i +TTX 1μM

HCRT1 100nM

2min
10pA

ii Baseline

+HCRT1 100nm

Wash

5pA
5s

iii

ΔmEPSC$_{HCRT-1}$ freq (%)

Time (min)

ΔmEPSC$_{HCRT-1}$ freq (%)

n.s.

BL HCRT W
(4) (4) (4)

A

MC

DTA

SD   RS

B

NRDE (µV²*h)

(4) (5) (3) (7)

SD   RS

c-FOS⁺ / nNOS⁺ (%)

■ MC
□ DTA

(3) (5) (3) (7)

SD   RS